Geochimica et Cosmochimica Acta 433 (2026) 71–90

Contents lists available at ScienceDirect

Geochimica et Cosmochimica Acta

journal homepage: www.elsevier.com/locate/gca

Source evolution controls the molybdenum isotope composition of Archean continental crust

Eric D. Vandenburg [a,b,c,*], Oliver Nebel [c,d], Laura M. Spencer [e,f], Marc-Alban Millet [f], R. Hugh Smithies [g,h], Peter A. Cawood [c], Alexandra Churchus [c], Wenli Liang [c], Emilie Bruand [i], Jean-François Moyen [j], Alex McCoy-West [k], Priyardarshi Chowdhury [l,m]

[a] Australian Critical Minerals Research Center, Department of Earth Sciences, School of Physics, Chemistry and Earth Sciences, Adelaide University, Adelaide, SA, 5005, Australia
[b] ARC Training Center in Critical Resources for the Future, Perth, WA, Australia
[c] School of Earth, Atmosphere and Environment, Monash University, Clayton, VIC, 3800, Australia
[d] GEOMAR Helmholtz Center for Ocean Research Kiel, Kiel, Germany
[e] Institut de Physique du Globe de Paris, Paris, 75005, France
[f] School of Earth and Environmental Sciences, Cardiff University, Cardiff, CF10 3AT, UK
[g] Department of Mines, Industry Regulation and Safety, Geological Survey of Western Australia, Perth, WA, 6004, Australia
[h] School of Earth and Planetary Sciences, Curtin University, Perth, WA, 6845, Australia
[i] Geo-Ocean Department, Université Bretagne Occidentale, CNRS, Plouzané, 29280, France
[j] Université Jean-Monnet, Laboratoire Magmas et Volcans, UCA-CNRS-IRD, Aubière, France
[k] IsoTropics Geochemistry Laboratory, Earth and Environmental Science, James Cook University, Townsville, QLD, 4811, Australia
[l] School of Earth and Planetary Sciences, National Institute of Science Education and Research Bhubaneswar, Odisha, India
[m] Homi Bhabha National Institute, Training School Complex, Mumbai, India

ARTICLE INFO

Associate Editor: Julie Prytulak

Keywords:
Molybdenum isotopes
Tonalite-trondhjemite-granodiorite (TTG)
Archean granitoids
Sanukitoids
Intracrustal reworking

ABSTRACT

Earth's continental crust is its most chemically evolved and diverse reservoir. Numerous studies have investigated its stable metal isotope character to understand its formation and secular evolution. Molybdenum (Mo) isotopes are useful tracers of petrogenetic processes in Phanerozoic igneous rocks, but Archean granitoids, which make up much of Earth's early continental crust, remain poorly characterized. Here, we report high-precision whole-rock Mo isotope data for 28 Archean granitoids from Australia's Pilbara and Yilgarn cratons, with crystallization ages from 3.52 to 2.63 Ga. The samples cover a spectrum of magmatic series, including tonalite-trondhjemite-granodiorite (TTG), TTG hybrid, sanukitoid, potassic, and potassic hybrid magmas.

After assessing the effects of alteration, crustal contamination, and fluid exsolution, we interpret the observed $\delta^{98/95}$Mo range of −0.93 to +0.25‰ as primarily reflecting magmatic source characteristics. TTG and TTG hybrid granitoids, together with samples derived from unenriched *meta*-mafic or mantle-like sources, have mean and median $\delta^{98/95}$Mo values close to, or slightly higher than, chondrite and depleted MORB mantle (DMM). In contrast, potassic, potassic hybrid, and sanukitoid series granitoids, as well as samples derived from enriched *meta*-mafic or felsic crustal sources, extend to lower, sub-mantle $\delta^{98/95}$Mo values.

Elemental proxy relationships, major- and trace-element modeling, and phase-equilibrium constraints indicate that source composition and residual mineralogy during partial melting primarily control Mo isotope variability in these rocks. In crustally-derived granitoids, lower $\delta^{98/95}$Mo values are associated with more mature source compositions and with changes in the abundance and composition of residual feldspar. Amphibole, garnet, and biotite may also have subordinate effects. These relationships suggest that Mo isotopes track the progressive reworking of Archean crust. Juvenile crust-derived TTG magmatism is characterized by near- to suprachondritic

* Corresponding author at: Australian Critical Minerals Research Center, Department of Earth Sciences, School of Physics, Chemistry and Earth Sciences, Adelaide University, Adelaide, SA 5005, Australia.

E-mail addresses: eric.vandenburg@adelaide.edu.au (E.D. Vandenburg), onebel@geomar.de (O. Nebel), spencer@ipgp.fr (L.M. Spencer), MilletM@cardiff.ac.uk (M.-A. Millet), hugh.smithies@dmirs.wa.gov.au (R.H. Smithies), peter.cawood@monash.edu (P.A. Cawood), alex.churchus@monash.edu (A. Churchus), Wenli.Liang@monash.edu (W. Liang), emilie.bruand@univ-brest.fr (E. Bruand), jean-francois.moyen@uca.fr (J.-F. Moyen), alex.mccoywest@jcu.edu.au (A. McCoy-West), priyadarshi@niser.ac.in (P. Chowdhury).

https://doi.org/10.1016/j.gca.2026.10.009
Received 12 December 2025; Accepted 6 October 2026
Available online 11 October 2026
0016-7037/© 2026 The Author(s). Published by Elsevier Ltd. This is an open access article under the CC BY license (http://creativecommons.org/licenses/by/4.0/).

$\delta^{98/95}$Mo, whereas later sanukitoid and potassic granitoid magmatism, linked respectively to mantle metasomatism and reworking of TTG-dominated gray gneiss, shifts toward lower $\delta^{98/95}$Mo values.

The observed trends imply that intracrustal reworking alone can push continental averages to sub-mantle values, with ramifications for mass-balance models. Although TTGs are generally suprachondritic, their $\delta^{98/95}$Mo values are not high enough to easily support models requiring large volumes of Hadean to Paleoarchean continental extraction from a chondritic mantle to offset the subchondritic Mo isotope composition inferred for the depleted mantle from Archean komatiites. The strong Mo isotope contrast between continental crust and upper mantle may therefore have developed after 2.6 Ga, once crustal recycling became more extensive.

1. Introduction

Continental crust formation began within the first Gyr of Earth's history. This early evolved crust was likely covered by water, with perhaps 30–80% of the present-day crustal volume reached by 3 Ga, as indicated by recent models (e.g., Korenaga and Spencer, 2025 and references therein). The growth of the planet's most evolved reservoir has led to the subaerial emergence of evolved crust and the exogenic interactions and element cycling that this entails (e.g., Smit and Mezger, 2017; Chowdhury et al., 2021; 2025; Lipp et al., 2021). Reconstructing the growth and evolution of early crustal reservoirs is difficult due to their partial preservation and subsequent tectonic overprints. The Archean continental crust is primarily comprised of granitoids, which, since 4 Ga, have intruded greenstone belts variably composed of basaltic lavas and subordinate shales and volcaniclastic sediments, equating to a calculated average andesitic composition (Rudnick and Gao, 2003; Kamber and Ossa Ossa, 2025). Understanding the early crust's extraction from the mantle and its evolution requires radiogenic isotopes, which trace time-integrated source evolution, alongside stable isotopes, which are sensitive to the mineralogy and conditions of magma generation. However, the stable isotope compositions of early crust remain poorly constrained for many elements, limiting our ability to reconstruct its evolution.

In cratons, which preserve the only direct records of the first two billion years of Earth's history, the granitoid component of the crust is (i) dominated by the high-Na, low-K tonalite-trondhjemite-granodiorite (TTG) series and (ii) the low-Na, high-K potassic series comprising granites, monzonites and syenites, with (iii) a subordinate contribution by the high-Mg, −Cr, −Ni and −LILE sanukitoid series. Each of these series is broadly characteristic of specific stages of a craton's formation and typically occurs in a common sequential order, a consequence of the changing tectonomagmatic environments accompanying their growth (e.g., Laurent et al., 2014; Cawood et al., 2018; Moyen and Laurent, 2018; Vandenburg et al., 2023a).

TTGs are the first granitoid series to appear in the lifecycle of a craton and are generally accepted to be the products of the anatexis of hydrated mafic protoliths (e.g., Rapp et al., 1991; Moyen and Martin, 2012; Palin et al., 2016; Tamblyn et al., 2023; Laurent et al., 2024), often (but not exclusively) due to the thickening of a mafic–ultramafic protocratonic plateau through volcanic resurfacing (e.g., Van Kranendonk et al., 2015; Chowdhury et al., 2021; Smit et al., 2024). Crucially, these magmas show little evidence for a direct or substantial mantle involvement in their petrogenesis (e.g., Smithies, 2000), reflecting a wholly crustally confined process. Their radiogenic isotopes, however, imply a relatively short crustal residence time for these sources, probably no more than 100–200 Myrs (e.g., Gardiner et al., 2021).

Later, sanukitoids appear, which are derived from sections of subprotocratonic mantle metasomatized by TTG/adakitic melts (Laurent, 2012; Spencer et al., 2024). This mantle metasomatism is generally interpreted as the result of delamination and foundering of the eclogitized lower crust of a plateau (Smithies et al., 2021) or by melting of a slab-like feature during a primitive subduction-like process (Smithies and Champion, 2000). Sanukitoids are usually the most spatiotemporally restricted of the three series (e.g., Laurent et al., 2014; Cawood et al., 2022), especially compared to TTGs.

Potassic granitoids generally appear last among the three main magmatic series in a craton (Cawood et al., 2022). Outside of isolated earlier occurrences comprising low melt fractions of *meta*-mafic sources (e.g., Gardiner et al., 2018), their presence reflects the reworking of composite "gray gneisses" comprised of earlier TTGs and subordinate supracrustal rocks (Moyen, 2011), often marking the incipient stabilization of a craton (Laurent et al., 2014; Cawood et al., 2018; Nebel et al., 2018).

Molybdenum (Mo) isotopes have gained considerable attention over the past decade, as studies have revealed substantial isotopic variation within- and between igneous rocks from different magmatic settings (e.g., Freymuth et al., 2015; Bezard et al., 2016; Yang et al., 2017; McCoy-West et al., 2019; Villalobos-Orchard et al., 2020; Hin et al., 2022; Willbold and Elliott, 2023; Zhao et al., 2025). Because Mo is both redox-sensitive and fluid mobile under oxidizing conditions, especially at lower temperatures (Kendall et al., 2017), Mo isotopes are strongly influenced by isotopic fractionation arising from seafloor alteration of the oceanic crust (Freymuth et al., 2015; Ahmad et al., 2021) and the dehydration of subducting slabs in subduction zones; the latter process of which produces isotopically heavy fluids and complementary isotopically light eclogites and anhydrous sediments (e.g., Freymuth et al., 2015; Gaschnig et al., 2017; Chen et al., 2019; Ahmad et al., 2021; Stegner et al., 2025). As such, Mo isotopes show utility in tracing the input of recycled components into the mantle, including in volcanic arcs (e.g., König et al., 2016; Villalobos-Orchard et al., 2020; Ahmad et al., 2022; Rojas-Kolomiets et al., 2023; Willbold and Messling, 2023; Liu et al., 2024), ocean island basalts (OIB; Gaschnig et al., 2021; Ahmad et al., 2023; Willbold and Elliott, 2023) and even mid-ocean ridge basalts (MORB; Chen et al, 2022b; Hin et al., 2022; Chen et al., 2025; Rodney et al., 2025). In contrast, nominally anhydrous partial melting of the mantle (e.g., at mid-ocean ridges) produces only limited Mo isotope fractionation (McCoy-West et al., 2019). In the crust, studies on granitoids have provided insights into the complexities of their petrogenesis. Initially, Mo isotope variations in granitoids were suggested to be dominated by source heterogeneity, perhaps modified by hydrous mineral crystallization (Yang et al., 2017; Chen et al., 2022a). Subsequent investigations have revealed the role of fluids in granitoids, which, if present during melting, result in melts with heavier $\delta^{98/95}$Mo than anhydrous melting (Fan et al., 2023; Zeng et al., 2024; Xia et al., 2025a, b), and if saturated in a closed magmatic system, can limit changes in $\delta^{98/95}$Mo arising from crystal fractionation (Fan et al., 2022).

The Mo isotope record of Archean magmatic systems remains limited; to date, only four studies have been conducted on mafic–ultramafic rocks: two on products of high degrees of deep mantle melting (i.e. komatiites: Greber et al., 2015; McCoy-West et al., 2019), yielding an average $\delta^{98/95}$Mo of -0.21 ± 0.06‰ (2 SD); and two others on melt products from cratonic metasomatized lithosphere: layered intrusions (Nebel-Jacobsen et al., 2021), yielding an average $\delta^{98/95}$Mo of -0.29 ± 0.16‰ (2 SD), and Neoarchean dykes (Chatterjee et al., 2025), with variable $\delta^{98/95}$Mo ranging from −0.27‰ to −0.04‰. Notably, none of these rock types likely represents typical shallow Archean mantle magmatism. Although much more common during this time, komatiites and layered intrusions were scarce even within cratons (e.g., Smith et al., 2024; Kamber and Ossa Ossa, 2025). Nevertheless, McCoy-West et al. (2019) used the $\delta^{98/95}$Mo compositions of Archean

komatiites to argue for present-day mantle depletion by 3.5 Ga, requiring the extraction of two times the modern volume of continental crust during the first billion years of Earth's history.

A vital, but underexplored aspect is the composition of the crustal products themselves: the Mo isotopic compositions of Archean granitoids remain essentially unknown. The only existing data come from two Fennoscandian TTG samples with disparate isotopic compositions (−0.10‰ and +0.21‰) analyzed by Greber et al. (2015), for which no trace element data are available, and a handful of TTGs from the Yangtze Craton (Liu et al., 2026), for which no geological reference materials were analyzed, making it impossible to evaluate the accuracy of the data (their results are therefore not discussed here). Understanding the composition of the early continental crust is crucial for assessing existing Mo isotope secular crustal extraction and recycling models, which use the crust-mantle isotopic contrast to estimate how much crust was extracted from the mantle and later recycled into it (McCoy-West et al., 2019; Tian et al., 2025). These have relied solely on inferences from Archean-Phanerozoic mafic–ultramafic rocks and Phanerozoic granitoids, with no data on the actual rocks for which the latter are invoked as a stand-in.

To address this gap, we present high-precision whole-rock molybdenum isotope data for a selection of well-characterized >3.52–2.63 Ga granitoids from the Pilbara and Yilgarn cratons of Western Australia. By analyzing samples from disparate intrusions, we provide a (multi) terrane-scale survey of the key craton building blocks, which we use to examine how magmatic processes and source influence the isotopic composition of Archean granitoids. This can provide insights into the Mo isotope composition of the early continental crust.

2. Samples and classification

The samples analyzed here are from the Paleo–Mesoarchean Pilbara Craton and Eo–Neoarchean Yilgarn Craton (Fig. 1), portions of the larger Western Australian Craton assembled during a series of Paleoproterozoic orogenies (Cawood and Korsch, 2008). Both cratons record protracted, widespread magmatic activity during the Archean and consist of amalgamated patchworks of distinct lithotectonic blocks, including some of the world's largest intact pieces of pre-3.2 Ga continental crust. We provide the geological histories of both cratons in the *Supplementary Information*.

These samples comprise a subset of the YiPi collection, an internally consistent, representative reference collection of granitoids and supracrustal rocks collected during a field campaign in September–October 2019. The samples come from unaltered outcrops previously characterized for geochemistry and geochronology by the Geological Survey of Western Australia (GSWA), from the same part of the outcrop when possible, or at least from the same phase/rock type. The sample set spans > 3.52 to 2.83 Ga in the Pilbara Craton and 2.96 to 2.62 Ga in the Yilgarn Craton (Geological Survey of Western Australia, 2020, 2021). Granitoids from the Pilbara Craton portion of the collection were previously characterized for whole-rock geochemistry and in situ Rb-Sr dating by Vandenburg et al. (2023a, b). The 28 samples analyzed cover the entire age range and compositional spectrum of the collection (Figs. 2 and 3).

We classify the samples in two ways: magmatic series and source affinity, using the ternary diagrams of Laurent et al. (2014) (Fig. 2b–c). Here, magmatic series is divided into the three main types of granitoids, TTG, potassic, and sanukitoid (*sensu lato*), along with their hybrids, using the Na_2O/K_2O – 2 ACNK (molecular $Al/[2Ca + Na + K]$) – 2 FMSB ($[FeO_t + MgO] \times [Sr + Ba]$, in wt.%) ternary diagram. At times in this study, we refer to TTGs and potassic granitoids (along with their hybrids, as these reflect the dominant component) as "crustally-derived granitoids", in that they are not associated with coeval mafic magmas and do not have a direct mantle source (following the "C-type" terminology of Moyen, 2020). The classification scheme employed here groups sanukitoids and sanukitoid-like rocks into a single series, "sanukitoid *sensu lato*." This partly reflects ambiguity in the definition of a sanukitoid (Spencer, 2025) and includes samples that other schemes would not classify as such (cf. Lowrey et al., 2023). There are two main types of hybrid: (i) purely crustally-derived and (ii) crust-mantle. Purely crustally-derived hybrids represent mixtures of TTG and potassic magmas or are derived from melting a source between these two endmembers (i.e., intermediate crust) (e.g., Laurent et al., 2014; Moyen, 2020). This has been used to explain the presence of "enriched" or "transitional" TTGs (Champion and Smithies, 2001). Crust-mantle hybrids reflect mixing and/or assimilation between mantle- and crust-derived melts/sources. For simplicity, we classify these samples based on the dominant magmatic series component, in this case either hybrid TTGs or potassic hybrids; further separation of these into purely crustally-derived and crust-mantle hybrids is beyond the scope of this study.

Source affinity is divided into five groups: low-K mafic rocks, high-K mafic rocks, mantle, felsic rocks, and sediments, based on the 3 CaO – A/FM ($Al_2O_3/[FeO_t + MgO]$) – 5 K_2O/Na_2O ternary first presented by Laurent et al. (2014) and subsequently presented in a modified form to accommodate the sources of more mafic endmembers in Laurent et al. (2019). The boundaries of this ternary are based on experimental studies of partial melting of various sources. We employ this ternary to assign the most likely dominant source component to our samples. It should be noted that the "mantle" field here represents a broadly mantle-like source; granitoids in this field may be derived from the mantle in part through fractional crystallization or mixing with mantle-derived magmas, or in some cases, represent a crustal source that is more primitive and perhaps less altered than the low-K mafic rock source, such as a gabbro.

These two classification schemes are not necessarily mutually inclusive; grouping them occasionally leads to unusual inferences (e.g., potassic granitoids derived from low-K mafic rocks). This arises from imposing distinct categorical boundaries upon a compositional spectrum, a perennial issue in granitoid geochemistry, and the occasional occurrence of lithologies with unique petrogeneses. The magmatic series and source affinity schemes represent only two of an infinite number of ways to classify our samples (c.f., Lowrey et al., 2023; Spencer, 2025). In our discussions, we treat magmatic series and source affinity separately to minimize contradiction.

2.1. Pilbara Craton granitoids

The granitoids from the Pilbara Craton ($n = 19$) range in age from 3.52 to 2.83 Ga and comprise every major granitoid supersuite from the craton (Hickman, 2023), except for the Railway and Elizabeth Hill supersuites (Fig. 1a). The sample suite is petrographically diverse, including two enclave specimens (see sample descriptions in Table S1). A primitive sanukitoid with 52.5 wt.% SiO_2 notwithstanding, their SiO_2 contents range from 59.9 to 77.0 wt.% and comprise CIPW-normative tonalites, trondhjemites, granodiorites, and granites belonging to the TTG, TTG hybrid, potassic, potassic hybrid, and sanukitoid (*s.l.*) magmatic series, with a diverse range of source affinities based on the classification schemes of Laurent et al. (2014) (Fig. 2, Fig. S1).

2.2. Yilgarn Craton granitoids

Granitoid samples from the Yilgarn Craton ($n = 9$) range in age from 2.95 to 2.63 Ga and are confined to the northwestern portion of the Youanmi Terrane, comprising the Bunnawarra, Rothsay, Big Bell, and Walganna Suites (Fig. 1b). In hand specimens, most samples are described as monzogranites or tonalites (see sample descriptions in Table S1). Geochemically, however, they are nearly as diverse as the Pilbara subset, with samples ranging from 63.9 to 74.4 wt.% SiO_2 that comprise CIPW-normative trondhjemites, granodiorites, quartz monzonites and granites. Their magmatic series and source affinities largely mirror those of the Pilbara, excluding TTGs and sediment-derived

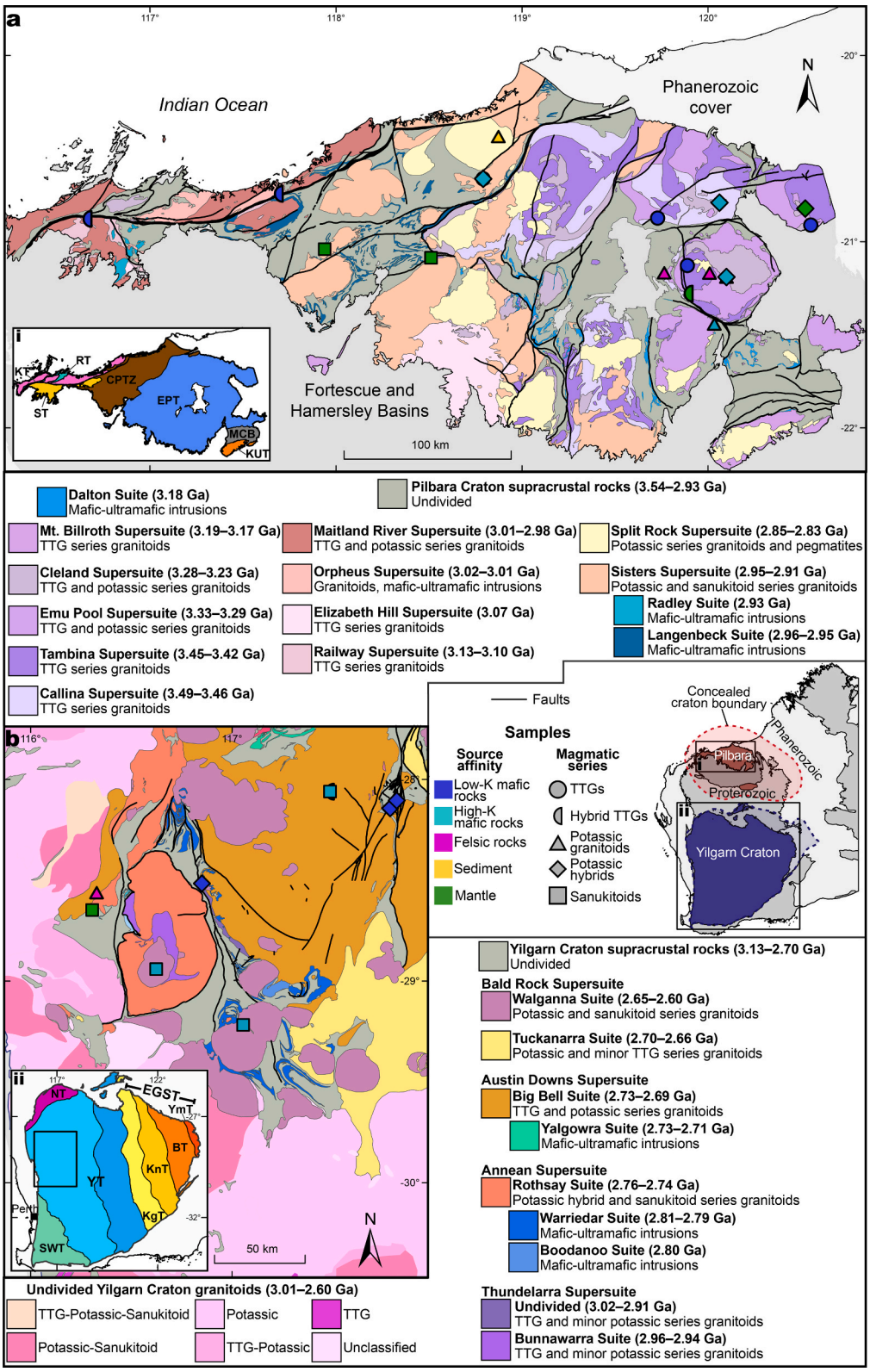


Fig. 1. Geological maps of the portions of the Western Australian Craton (WAC) involved in this study, showing sample localities. The inset shows the total extent of the exposed and concealed portions of the Pilbara and Yilgarn cratons within the WAC. (a) Geological map of the exposed portion of the Pilbara Craton. Inset i displays the lithotectonic subdivisions of the exposed portion of the craton. CPTZ – Central Pilbara Tectonic Zone; EPT – East Pilbara Terrane; KT – Karratha Terrane; KUT – Kurrana Terrane; MCB – Mosquito Creek Basin; RT – Regal Terrane; ST – Sholl Terrane. (b) Geological map of the studied northwestern portion of the Younami Terrane of the Yilgarn Craton, illustrating the spatial distribution and affinities of granitoid supersuites and mafic–ultramafic intrusive suites. Inset ii displays the lithotectonic subdivisions of the Yilgarn Craton. BT – Burtville Terrane; EGST – Eastern Goldfields Superterrane; KgT – Kalgoorlie Terrane; KnT – Kurnalpi Terrane; NT – Narryer Terrane; SWT – South West Terrane; YT – Youanmi Terrane; YmT – Yamarna Terrane. Maps were constructed using shapefiles from the Geological Survey of Western Australia (2021).

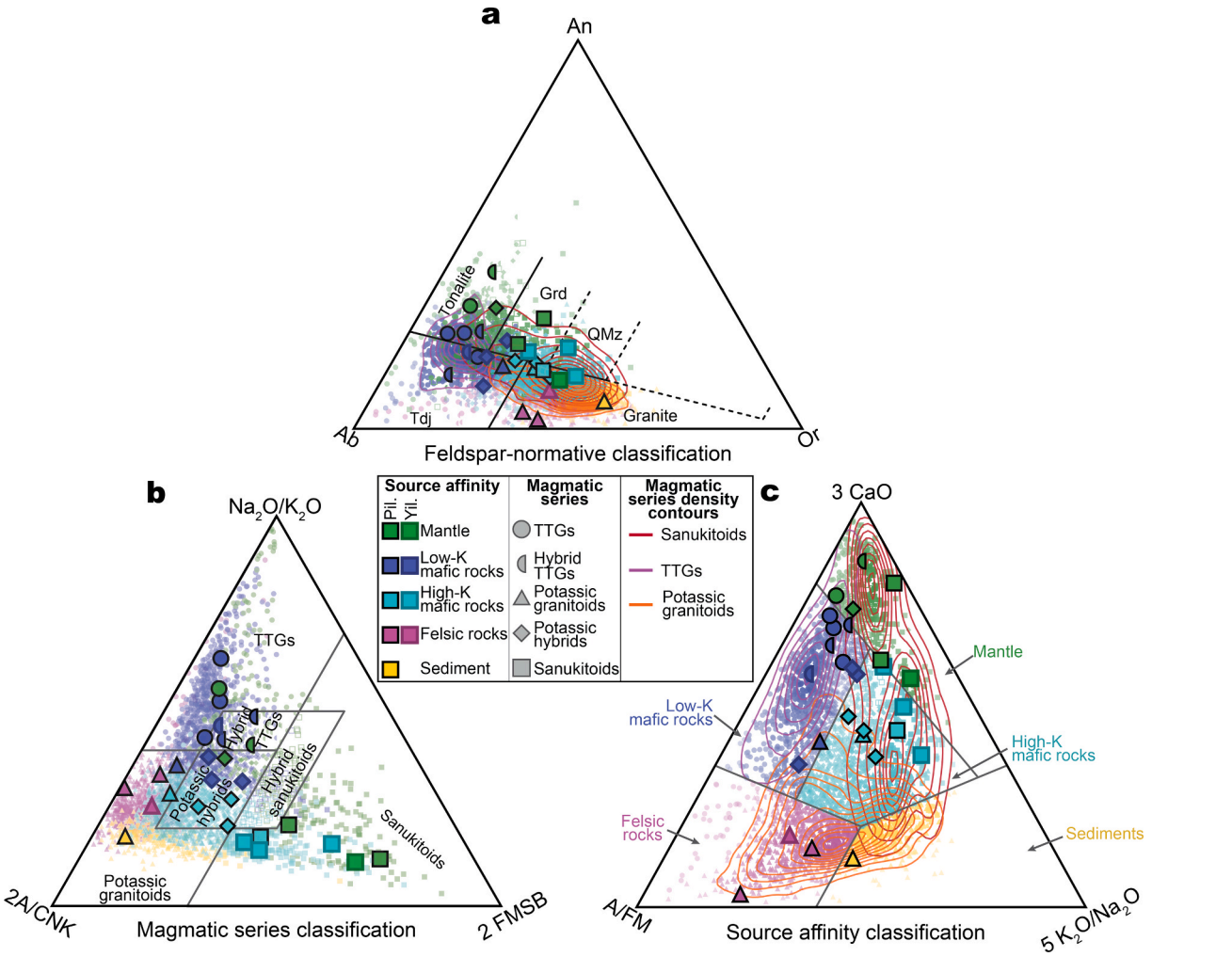


Fig. 2. Geochemical classifications of studied samples and their representativeness of Eo–Neoarchean granitoids from the Pilbara and Yilgarn Cratons. (a) CIPW-normative feldspar classification ternary of O'Connor (1965). (b) Magmatic series classification ternary of Laurent et al. (2014, 2019). (c) Source affinity classification ternary of Laurent et al. (2014). A/CNK = molecular Al/(2Ca + Na + K); A/FM = Al_2O_3/(FeO_t + MgO); FMSB = (FeO_t + MgO) × (Sr + Ba) (in weight percent). Samples analyzed in this study are represented by larger symbols with outlines; smaller symbols correspond to data compiled from the Yilgarn (Lowrey et al., 2023) and Pilbara (Vandenburg et al., 2023a) cratons. Density contours for each magmatic series endmember in (a) and (c) are calculated using the compiled data. Grd – granodiorite; QMz – quartz monzonite; Tdj – trondhjemite.

granitoids, respectively (Fig. 2, Fig. S1).

3. Methods

3.1. Sample preparation

Very large representative samples, generally ~ 3–5 kg, were collected from unaltered outcrops and cleaned in the field as much as possible to remove weathering rinds. To minimize contamination during preparation at Monash University (Clayton, Australia), samples were cleaned by trimming off the remaining weathering rinds with a diamond blade saw, rinsed with deionized water, removed of metal abrasion, crushed with a ceramic jaw crusher and disc crusher, and finally milled in an agate ring mill. These powders were used for whole-rock major, minor and trace element, and Mo isotope analyses. Whole-rock major, minor and trace element geochemical analyses were conducted at ALS Minerals, Perth, Western Australia, as previously described in Vandenburg et al. (2023a).

3.2. Mo isotope analysis

Rock powder digestion, Mo purification and Mo isotope analysis were performed at the School of Earth, Atmosphere and Environment, Monash University. Molybdenum isotope compositions were determined using a double-spike MC-ICP-MS technique following Archer and Vance (2008), with Mo separation following Willbold et al. (2015).

To minimize contamination, we undertook sample digestion and Mo purification in an ISO-4 clean laboratory using double-distilled acids. We adopted a two-stage procedure combining hotplate and microwave digestion to ensure complete dissolution of refractory minerals such as zircon. Depending on Mo concentrations, 100–1100 mg of sample powder, targeting 100–220 ng of Mo, was weighed out and mixed with a ^{97}Mo-^{100}Mo double spike solution in a 1:1 M proportion of Mo in the sample-spike mixture, then digested in a 4:4:1 mixture of concentrated HF-HNO_3-HCl. Residues were repeatedly taken up in 6 M HCl and treated with aqua regia to dissolve precipitated fluorides, before being dissolved in 3 M HCl with ascorbic acid added to reduce iron to its ferrous state. Molybdenum was then separated from the matrix and interfering elements by single-column anion exchange chromatography using BioRad AG1x8 100–200 mesh resin, following Willbold et al. (2015). Samples were treated with an HNO_3-H_2O_2 mixture to eliminate organic residue and taken up in 0.32 M HNO_3-0.28 M HF for analysis. Full details of the digestion and purification procedures, including reagent volumes, temperatures and durations, are given in the

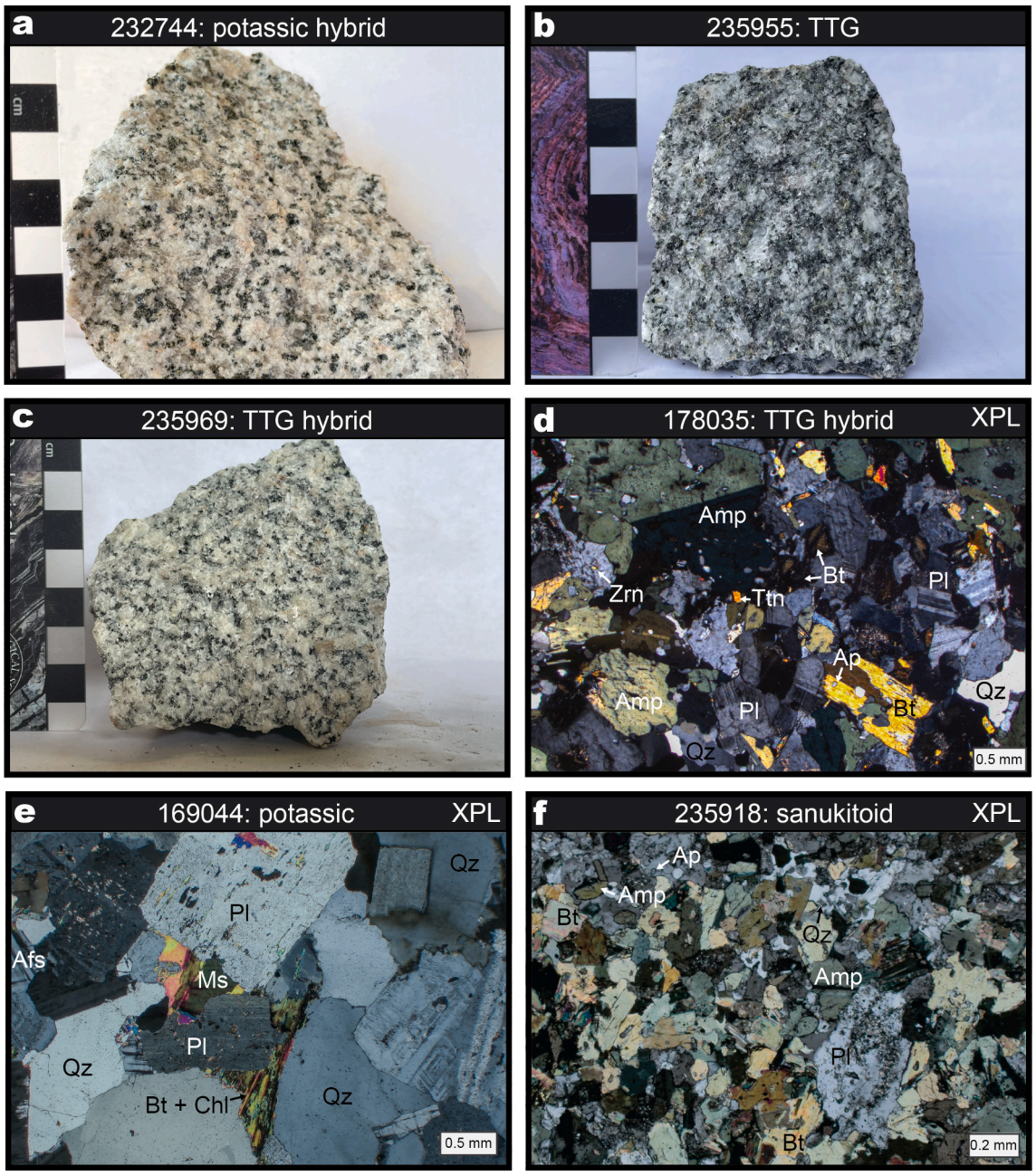


Fig. 3. Hand sample photographs (a–c) and photomicrographs (d–f) of selected samples analyzed in this study. The samples in this study largely retain their primary mineralogy and igneous textures. Afs – alkali feldspar; Amp – amphibole; Ap – apatite; Bt – biotite; Chl – chlorite; Ms – muscovite; Pl – plagioclase; Qz – quartz; Ttn – titanite; Zrn – zircon.

Supplementary Methods.

Molybdenum isotopic analyses were performed on a Thermo Scientific™ Neptune*Plus*® MC-ICP-MS connected to a Cetac® Aridus II desolvating nebulizer system with a ca. 50 μL/min aspiration rate in static, low-resolution mode under dry plasma conditions. Six Mo isotopes (^{94}Mo, ^{95}Mo, ^{96}Mo, ^{97}Mo, ^{98}Mo, and ^{100}Mo) were measured concurrently with ^{99}Ru and ^{101}Ru to monitor potential isobaric interferences. Measurements of each sample, diluted to 62–90 ppb concentrations, were bracketed by measurements of spiked 75 ppb NIST SRM 3134 solutions (within 20% of unknowns), typically corresponding to a ^{98}Mo intensity of 2.5 V on a 10^{11} Ω amplifier. Individual measurements consisted of 60 s uptake, followed by 35 cycles (for samples analyzed twice) and 70 cycles (for samples analyzed once) of 4.194 s integration time, and a 4-minute washout in a 0.32 M HNO_3-0.28 M HF wash solution. Data reduction utilized an offline MATLAB script, based on the double-spike deconvolution procedure of Rudge et al. (2009). All ^{98}Mo/^{95}Mo isotope data are presented as permil deviations from the NIST SRM 3134 Mo reference material (Greber et al., 2012):

$$\delta^{98/95}Mo(‰) = \left[\frac{\left(^{98}Mo/^{95}Mo\right)_{sample}}{\left(^{98}Mo/^{95}Mo\right)_{NIST3134}} - 1\right] \times 1000$$

Mo concentrations were calculated via the double spike isotope dilution method. Total procedural blanks of 0.16 and 0.40 ng translate to < 1% blank contributions for all samples, with blank-corrected and uncorrected data identical within uncertainty (we present the latter in all tables and figures). Repeated measurements of NIST SRM 3134 and an in-house J&M standard solution (JMCBern) over two years gave an isotopic difference of $\Delta^{98/95}$Mo = 0.268 ± 0.045‰ (2 SD, n = 20), in

agreement with previous studies (Greber et al., 2012; Ahmad et al., 2021, 2022, 2023; Kaufmann et al., 2021). Repeated digestions of whole-rock reference materials USGS AGV-2 (andesite) and W-2a (diabase) yielded $\delta^{98/95}$Mo of −0.16 ± 0.06‰ (2 SD, number of digestions [n] = 2, number of runs [N] = 6); and −0.06 ± 0.05‰ (2 SD, n = 3, N = 6) (Table S2), which are within uncertainty of previously determined values (Table S3; e.g., Willbold et al., 2015; Villalobos-Orchard et al., 2020; Ahmad et al., 2021; Nebel-Jacobsen et al., 2021; Hin et al., 2022; Rojas-Kolomiets et al., 2023; Pontow et al., 2025). We assign a 2 SD uncertainty for our unknown samples using the most conservative reproducibility of ± 0.06‰, based on the repeat analysis of W-2a. Individual digestions of whole-rock reference materials USGS BIR-1 (basalt) and GSJ JB-2 (basalt) are also within this reproducibility and yielded $\delta^{98/95}$Mo of − 0.11 ± 0.01‰ (2 SE_m, N = 1) and 0.08 ± 0.01‰ (2 SE_m, N = 1) (Table S2), in line with previously determined values (Table S3; e.g., Burkhardt et al., 2014; Willbold et al., 2015; McCoy-West et al., 2019; Villalobos-Orchard et al., 2020; Hin et al., 2022; Willbold and Messling, 2023; Pontow et al., 2025). We obtained average Mo concentrations of 1.728 ± 0.008 μg/g (2 SD, n = 2) and 0.379 ± 0.008 μg/g (2 SD, n = 3) for AGV-2 and W-2a, respectively. These concentrations are lower than the compiled values of Jochum et al. (2016) but agree with published values from other Mo isotope studies (see above references for $\delta^{98/95}$Mo).

4. Results

Table S1 presents the molybdenum contents and isotopic compositions of the Pilbara and Yilgarn granitoids alongside whole-rock geochemistry. The granitoids exhibit a large range in $\delta^{98/95}$Mo between −0.93‰ and +0.25‰ (n = 28; Table S1), which is both lighter

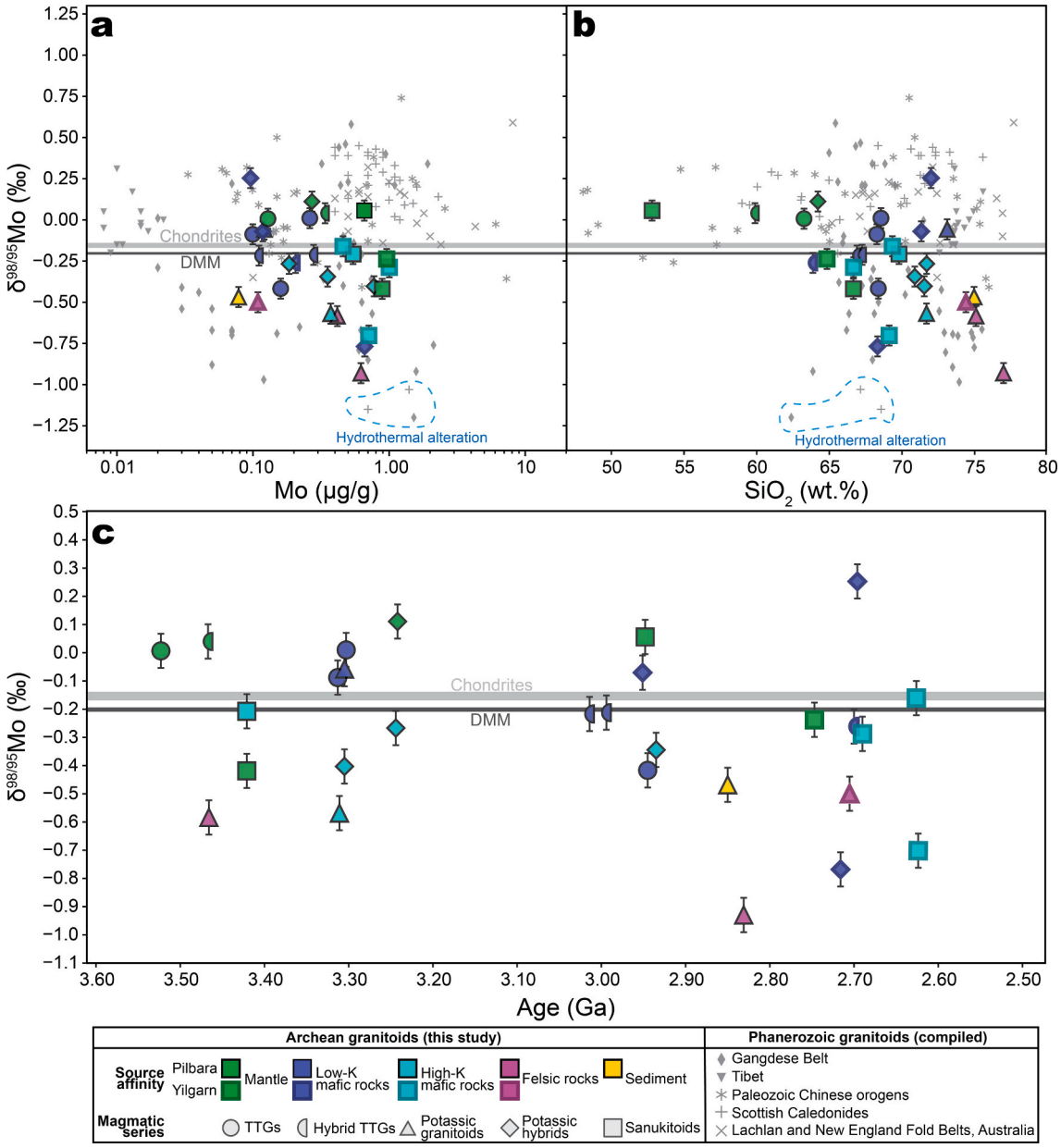


Fig. 4. Molybdenum isotope ratios vs. Mo (a) and SiO_2 (b) contents of Archean (this study) and Phanerozoic (compiled) granitoids, and Mo isotope ratios of Archean granitoids vs. sample age. The dark gray band represents the estimated $\delta^{98/95}$Mo composition of the depleted MORB mantle (DMM) from Hin et al. (2022), whereas the light gray band represents the $\delta^{98/95}$Mo composition of chondrites from McCoy-West et al. (2019). Error bars indicate 2 SD external reproducibility on our samples. Gangdese Belt data are from Fan et al. (2022, 2025); Tibet data are from Fan et al. (2021); Paleozoic Chinese orogens data are from Chen et al. (2022a), Fan et al. (2022), and Xia et al. (2025a, b); and Scottish Caledonides, Lachlan Fold Belt and New England Fold Belt data are from Yang et al. (2017).

and heavier than estimates of the depleted mantle (−0.22‰ to −0.20‰; McCoy-West et al., 2019; Hin et al., 2022), but well within the range observed in Phanerozoic granitoids and adakites (Figs. 4 and 5). The same variability extends to the craton scale, with samples from the Pilbara Craton ranging from −0.93‰ to +0.11‰ ($n = 19$), and samples from the Yilgarn Craton ranging from −0.77‰ to +0.25‰ ($n = 9$). This Mo isotope variability is also moderately associated with SiO_2 content (Spearman's $\rho = -0.446$, $p = 0.0173$; Fig. 4b).

Molybdenum isotope compositions vary systematically with source affinity, with mean and median $\delta^{98/95}$Mo increasing in the order felsic rocks < high-K mafic rocks < low-K mafic rocks < mantle (Fig. 5). Granitoids with felsic ($n = 3$) and high-K mafic ($n = 8$) source affinities are lighter than depleted mantle on both measures, whereas those with low-K mafic ($n = 10$) and mantle-like ($n = 6$) affinities are heavier. Differences between magmatic series are less pronounced, but in the same sense, with mean and median $\delta^{98/95}$Mo increasing from potassic granitoids through the potassic hybrid and sanukitoid series to hybrid TTGs and TTGs, although the relative positions of potassic hybrids and sanukitoids differ between mean and median. While still variable, the potassic ($n = 6$) and sanukitoid ($n = 7$) series granitoids have mean and median $\delta^{98/95}$Mo that are lighter than depleted mantle, whereas potassic hybrid ($n = 7$) samples have median $\delta^{98/95}$Mo lighter than depleted mantle and mean indistinguishable from it (Fig. 5). TTG series granitoids ($n = 4$) have mean and median $\delta^{98/95}$Mo heavier than depleted mantle. TTG hybrids ($n = 4$) are also indistinguishable from depleted mantle, with a median of −0.215‰ and a heavier mean reflecting a single sample at + 0.04‰ (Fig. 5). There is no apparent temporal trend in Mo isotope compositions, either within each craton or combined (Fig. 4c). Molybdenum contents are low but heterogeneous, ranging from 0.078 to 1.004 μg/g and generally highest in sanukitoids (Fig. 4a).

5. Discussion

5.1. Effects of post-emplacement alteration

Molybdenum is a fluid-mobile element; hence, its isotope signature is susceptible to modification by low-temperature fluids and post-emplacement processes, such as chemical weathering (McCoy-West et al., 2019; Gaschnig et al., 2021). Preferential aqueous mobilization of Mo^{6+} during chemical weathering releases isotopically heavy Mo, shifting a rock's isotopic composition to lighter values. Hydrothermal fluids may also change Mo isotope compositions, but the effect is not particularly straightforward and can shift $\delta^{98/95}$Mo to both lighter and heavier values (Greber et al., 2014; Neely et al., 2018; Kaufmann et al., 2021; Bezard and Guo, 2023). Supercritical hydrothermal fluids are particularly important to granitoid systems (Bezard and Guo, 2023). Preferential partitioning of isotopically heavy Mo into such fluids can drive residual granitoids to ultralight $\delta^{98/95}$Mo (< −1.00‰) during secondary alteration, as observed in the Fleet and Loch Doon plutons of Scotland (Yang et al., 2017) (Fig. 4). The mechanism is discussed further in the *Supplementary Information*.

Our samples come from a reference collection that avoided sampling areas with pervasive alteration and veining to ensure original magmatic compositions. Their Chemical Index of Alteration (CIA; Nesbitt and Young, 1982) values fall between 45.1 and 53.1, within the range expected for fresh granitoids (~45–55), except for primitive sanukitoid 235918 (CIA = 38.7), which, at 52.8 wt.% SiO_2 lies within the range expected for fresh mafic rocks (~30–45) (Fig. S2b). Consistent with this,

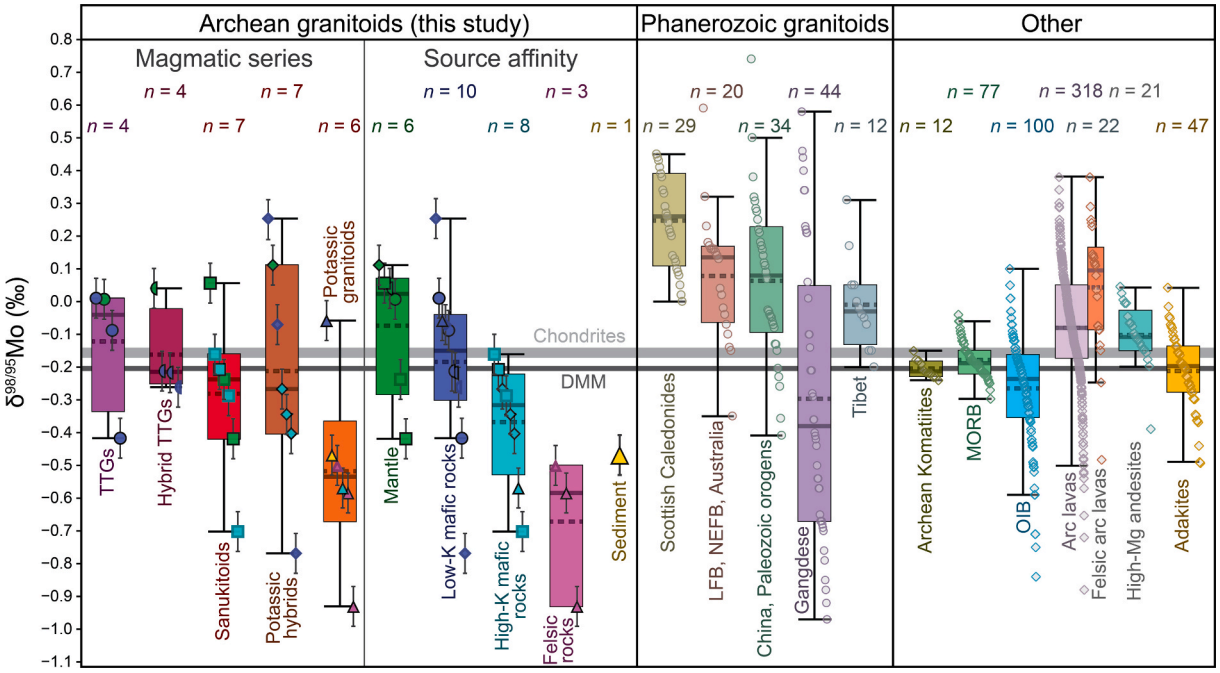


Fig. 5. Molybdenum isotopic variations in Archean granitoids from this study and Phanerozoic granitoids and selected Archean and modern mantle-derived rocks from the literature. $\delta^{98/95}$Mo variation exists both within and between magmatic series, with portions of their interquartile ranges overlapping with each other, as well as with chondrites (light gray band; McCoy-West et al., 2019) and depleted MORB mantle (DMM; Hin et al., 2022) for all series other than potassic granitoids. Potassic granitoids, albeit variable, generally exhibit the lowest $\delta^{98/95}$Mo, resembling Cenozoic granitoids from the Gangdese Belt. However, source affinity appears to exert the dominant control on Archean granitoids, with mean, median and interquartile bound values decreasing from mantle-derived to felsic rock-derived granitoids. Only the interquartile range of the mantle and low-K mafic rock affinity groups overlap in $\delta^{98/95}$Mo with chondrites and/or DMM. Sample symbols as per Figs. 2 and 3. The box on each group defines the 25th–75th percentiles (interquartile range; IQR), while the enclosed solid and dashed lines denote the median and mean values, respectively. Whiskers are 1.5 times the IQR. Phanerozoic granitoid data are compiled from the same sources as Fig. 4 (Table S11). Archean komatiite data are compiled from Greber et al. (2015) and McCoy-West et al. (2019); MORB data are compiled from Bezard et al. (2016), Chen et al. (2022b), Ahmad et al. (2022), and Hin et al. (2022) (Table S12); ocean island basalt (OIB) data is from the compilation of Fang et al. (2023); compiled arc lavas and their references are provided Table S13; high-Mg andesite data is compiled from Liu et al. (2024) and Zeng et al. (2025); and adakite data is compiled from Bezard et al. (2023), Liu et al. (2023), Rojas-Kolomiets et al. (2023), Liu et al. (2024), and Zeng et al. (2024) (Table S13).

all samples plot on the igneous trend of the Mafic-Felsic-Weathered (MFW) diagram of Ohta and Arai (2007) (Fig. S2a), and within the expected region of the Chlorite-Carbonate-Pyrite Index (CCPI) versus Ishikawa Alteration Index (AI; Ishikawa et al., 1976) diagram of Large et al. (2001) (Fig. S2c). Loss on ignition (LOI) contents are correspondingly low (<2.5 wt.%, with 20 of 28 samples below 1 wt.%), indicating minimal growth of secondary hydrous minerals, particularly given that some LOI is intrinsic to the hydrous mineralogy of most granitoids (e.g., Clemens, 1984; Whitney, 1990).

In the Pilbara, the granitoid complexes experienced unroofing around 400–350 Ma (Morón et al., 2020) and in the Yilgarn after 315 Ma (Veevers et al., 2005; Weber et al., 2005). Thus, we must rule out oxidative alteration, particularly oxidative weathering. The insignificant Ce anomalies ($Ce/Ce^* = 0.786–1.089$; $Ce_N/\sqrt{[La_N \times Pr_N]}$; normalized to primitive mantle of Palme and O'Neill, 2013) in our samples suggest minimal, if any, oxidative alteration. Furthermore, systematic relationships between Ce/Ce* and Mo/Nb (Fig. S2d) are absent, suggesting no alteration-controlled oxidation has redistributed Mo in our samples.

The third line of evidence comes from the Mo isotope signatures of our samples and their lack of an appreciable relationship with the aforementioned geochemical proxies of alteration and weathering. Our granitoids exhibit $\delta^{98/95}Mo > -1.00‰$, heavier than isotopic signatures in previously documented hydrothermally-altered granitoid occurrences, which can be as light as −1.73‰ (e.g., Yang et al., 2017; Fan et al., 2022). Second, molybdenum isotope compositions show no statistically significant relationship with LOI ($\rho = 0.25$, $p = 0.20$, $n = 28$) or CIA (Spearman's $\rho = -0.36$, $p = 0.06$, $n = 27$; note 235918 excluded, as above; Fig. S2e–f). Nor could the weak covariation with CIA plausibly represent an alteration signal: our granitoids span only 8 CIA units, and none exceeds 53.1, whereas the Ca, Na and K loss needed to drive $\delta^{98/95}Mo$ lighter through chemical weathering would push CIA tens of units higher, towards clay-rich shale compositions (~70–75).

5.2. Late-stage fluid exsolution and removal

During differentiation, silicate magmas become increasingly enriched in volatile components, such as H_2O, F, Cl, and B, which behave incompatibly (e.g., Wyllie, 1979; Williams-Jones and Heinrich, 2005; Dolejš and Zajacz, 2018; Audétat and Edmonds, 2020). Fluid saturation occurs in response to fractional crystallization and decreasing pressure, leading to the exsolution of an aqueous fluid phase (Thomas et al., 2005; Heinrich and Candela, 2013; Wilkinson, 2013). Molybdenum is preferentially transported in hydrothermal fluids (Candela and Holland, 1984; Zajacz et al., 2008; Tattich and Blundy, 2017), so this separation process could deplete Mo relative to similarly incompatible fluid-immobile elements in granitoids, as observed in some plutonic suites (Greaney et al., 2018). The *Supplementary Information* provides an in-depth discussion of the contradictory consequences of fluid exsolution on Mo isotopes inferred from the literature.

Because the samples in our dataset are not genetically related, tracing the effects of fluid exsolution is difficult, as each sample is likely derived from parental melts with different sources and geochemical signatures. However, several source-insensitive geochemical proxies can assess fluid exsolution and its impact on Mo isotopes. Zirconium and hafnium have identical valence and similar ionic radii, and thus behave similarly during magmatic differentiation (Louvel et al., 2014); Zr/Hf of 26 to 46, within the charge-and-radius-controlled field, is characteristic of magmatic systems (Bau, 1996). However, exsolution of F-rich fluids during extreme fractionation of (typically peraluminous) granitic magmas can significantly decouple Zr and Hf, pushing Zr/Hf to low values outside the charge-and-radius-controlled field due to compatibility differences (Bau, 1996; Wilke et al., 2012). Fluid exsolution can also be evaluated by examining the degree of the lanthanide tetrad effect ($TE_{1,3}$); that is, the shape (convexity vs concavity) of the rounded divisions of the first (La–Nd) and third (Gd–Ho) tetrads (Irber, 1999). A $TE_{1,3}$ value > 1.1 defines the tetrad effect threshold, observed during the final stages of extreme granitic magma evolution, where a highly evolved residual melt coexists with high-temperature magmatic-derived fluids (Irber, 1999). Twenty-seven of our 28 samples exhibit magmatic Zr/Hf (26–46) coupled with $TE_{1,3}$ below the threshold of 1.1 (Fig. S3a). The exception, 169044, has Zr/Hf of 14 and $TE_{1,3}$ of 1.16, and is also our lightest sample ($\delta^{98/95}Mo = -0.93‰$; Fig. S3b). This sample records fluid exsolution, although these indices alone cannot establish whether its Mo isotope composition was modified as a result. We retain it because it is from the Moolyella Monzogranite, a highly fractionated granite associated with pegmatite-hosted Sn-Ta mineralization (Hickman, 2023); such autometasomatized, rare-metal-bearing granites are a characteristic terminal product of Archean potassic magmatism rather than an aberration. To ensure this uncertainty does not impact our conclusions, we report all correlation statistics both with and without this sample (Table S4). The remaining 27 samples show no evidence of fluid exsolution, including a lack of correlation with alteration indices (Section 5.1) and between $\delta^{98/95}Mo$ and Ba/Nb (Fig. S3c); their Mo isotope compositions are therefore magmatic. The same is likely true of 169044, though this cannot be established independently.

5.3. Effect of magmatic processes on Mo isotope compositions of Archean granitoids

Like fluid exsolution, evaluating the impacts of crustal contamination and fractional crystallization on the Mo isotope compositions of our granitoids is complicated because the samples are not genetically related. An added complexity is the crustally-derived nature of the TTG and potassic series (e.g., Moyen, 2020), such that many of the minerals that crystallize out of the melts are also the minerals that comprise significant proportions of their source protoliths (e.g., amphibole, plagioclase, quartz, and biotite, ± alkali feldspar if the source is comprised of felsic crust) and adjacent country rocks (e.g., Moyen and Martin, 2012; Johnson et al., 2017; White et al., 2017; Rollinson, 2021). Below, we disentangle the effects of crustal contamination and fractional crystallization on the Mo isotope compositions of our granitoids.

5.3.1. Crustal contamination

Crustal assimilation features in many granitoid plutons (e.g., Clemens and Stevens, 2016; Moyen et al., 2021a, b) and can potentially modify magmatic Mo isotope compositions. Our sampling cannot exclude it directly, but several considerations suggest it is unlikely to account for the between-group differences we observe. The samples investigated here span nearly 1 Ga of Earth's history across two cratons, so any contaminants would be expected to vary widely in composition; producing the systematic differences between source affinity groups seen in Fig. 5 would require contamination that was correspondingly systematic in space and time. Moreover, the compositions of crustally-derived granitoids reflect the crust they are derived from, including the assimilant.

Two further considerations apply to the crustally-derived granitoids (TTGs, potassic granitoids and their hybrids). First, crustally-derived granitoid magmas generally sit close to their solidus, and the heat required to assimilate country rocks efficiently would freeze the melt (Roberts and Clemens, 1995; Glazner, 2007). Second, in the specific case of Archean crustally-derived granitoids, the available contaminant is compositionally close to either the source of the magma in the early stages of craton formation (e.g., amphibolites) or to the magma itself in the later stages (e.g., TTG-dominated felsic crust; e.g., Hoffmann et al., 2019; Moyen, 2020).

For the sanukitoids, which have the highest Mo concentrations of the five magmatic series, the direction of any contamination effect argues against it. Molybdenum contents in these samples do not change significantly with magnesium number (Mg#; Fig. S4a). Mg# shows a moderate correlation with $\delta^{98/95}Mo$ (Spearman's $\rho = 0.49$; Fig. S4b), but the potential assimilants (e.g., TTGs) have lower Mo concentrations and

generally heavier Mo isotope compositions than the sanukitoids (Fig. 4a and 5), so substantial contamination would be required to shift their Mo isotope compositions, which would be towards heavier rather than lighter values. Source composition therefore remains the more parsimonious explanation for the Mo isotope systematics of our granitoids.

5.3.2. Fractional crystallization

We thoroughly discuss the literature constraints on Mo isotope fractionation during fractional crystallization in the Supplementary Discussion. However, mineral–melt fractionation of Mo isotopes in magmatic systems remains poorly constrained because no targeted experimental studies exist, and the only available $\Delta^{98/95}Mo_{mineral\text{-}melt}$ estimates (biotite and amphibole from Kos; Voegelin et al., 2014) are debated and may not be widely applicable. On this limited basis, it is commonly inferred that hydrous calc-alkaline magmas evolve toward heavier Mo isotope compositions as amphibole and biotite fractionate from the melt, whereas tholeiitic magmas do not (e.g., Voegelin et al., 2014; Yang et al., 2015; Willbold and Elliott, 2017; Wille et al., 2018; Nebel-Jacobsen et al., 2021; Pontow et al., 2025). This is attributed to preferential incorporation of light Mo isotopes into hydroxyl-bearing octahedrally-coordinated sites in amphibole and biotite, relative to tetrahedrally-coordinated Mo^{6+} in the silicate melt (Ghose, 1965; Farges et al., 2006a; Voegelin et al., 2014; Wille et al., 2018), although the fractionation factors remain uncertain. In contrast, studies of Gangdese granites show decreasing $\delta^{98/95}$Mo with increasing SiO_2 that correlates with feldspar fractionation, consistent with feldspar, biotite and magnetite separates commonly having $\Delta^{98/95}Mo_{mineral\text{-}whole\ rock} > 0‰$ (Fan et al., 2021, 2022). This implies that heavy Mo isotopes may be preferentially partitioned into crystalline phases in highly polymerized, high-SiO_2, volatile-rich magmas, and drive the residual melt toward lighter $\delta^{98/95}$Mo (Farges et al., 2006a, b; Fan et al., 2021, 2022).

These contrasting behaviors are further complicated by the open-system nature of granitoid plutons, which consist of evolving crystal mushes and mixed melts rather than true liquids. Crystals form over protracted intervals and are only intermittently segregated from melt and thus may display Mo isotope disequilibrium with their host rocks and with one another (e.g., Lee and Morton, 2015; Bachmann and Huber, 2016, 2019; Holness, 2018; Deng et al., 2021; Fan et al., 2022; Bezard et al., 2023; Bucholz, 2025). Consequently, bulk-rock $\delta^{98/95}$Mo in granitoids typically reflects an amalgam of minerals with diverse isotopic histories mixed with residual interstitial melt, which can obscure systematic signals of fractional crystallization.

Each intrusive phase studied here is represented by a single sample, and since the groups are neither cogenetic nor comagmatic, we cannot assess the effects of fractional crystallization within suites. We therefore cannot exclude fractional crystallization based on within-suite systematics, and note only that we find no positive evidence for it; $\delta^{98/95}$Mo does not show a clear correlation with F, the proxy for amphibole and feldspar fractionation devised by Smit et al. (2024) ($10 - ([Nb - 8]/[Ti/Ti^* - 1]$, where $Ti/Ti^* = Ti_N/\sqrt{[Zr_N \times Gd_N]}$, normalized to primitive mantle of Hofmann, 1988) (Fig. S4d), and the magmatic groups deviate from the Zr vs SiO_2 evolutionary trend expected for closed-system differentiation (Lee and Bachmann, 2014; Fig. S4c). Together with the crystal mush processes discussed above, which tend to obscure rather than preserve fractionation signals, this leads us to favor source variation as the explanation for the between-group differences in $\delta^{98/95}$Mo.

5.3.3. No evidence for Mo isotope control by sulfides or Fe-Ti oxides

Sulfides are unlikely to influence the Mo isotope compositions of our samples, whether present in the source or formed by sulfur saturation of the magma during ascent. Magmatic sulfides (e.g., pyrrhotite, chalcopyrite) are not significant Mo hosts, likely because Mo is not sufficiently reduced (O'Neill and Eggins, 2002; Greaney et al., 2018; Neely et al., 2018). We nonetheless test this expectation because a phase need not be a major host to impart an isotopic signature; biotite, hornblende and garnet contain little Mo yet have been proposed to exert mineralogical controls on granitoid $\delta^{98/95}$Mo (Yang et al., 2017; Fan et al., 2022). Sulfide is the principal host of Cu in granitoids, so bulk Cu contents track the sulfide component; $\delta^{98/95}$Mo would be expected to covary with Cu if sulfide exerts control. No such relationship exists (Spearman's $\rho = 0.06$, $p = 0.78$; Fig. S5a), across Cu contents spanning more than two orders of magnitude (0.58–126 μg/g). Furthermore, immiscible sulfide phase separation would generate a positive correlation between Cu/Mo and Mo/Ce, since compatibility in a sulfide melt decreases Cu > Mo > Ce (Ma et al., 2022); no such correlation is observed (Spearman's $\rho = -0.05$; Fig. S5b).

The most important Mo-bearing phases in granitoids are titanite and Fe-Ti oxides, such as magnetite, ilmenite, and rutile (Greaney et al., 2018). Due to its similar ionic radius, octahedrally-coordinated Mo can be incorporated in its hexavalent state in the Ti^{4+} site via coupled substitution (e.g., $Ti^{4+} \leftrightarrow Fe^{3+}$; Shannon, 1976; Willbold and Elliott, 2017; Greaney et al., 2018), or, if locally reduced to Mo^{4+}, isovalently substitutes for Ti^{4+} (Zack et al., 2002; Skora et al., 2017; Prytulak and König, 2025). Thus, in principle, Ti-bearing phases may fractionate the Mo isotope compositions of melts (Chen et al., 2019). However, multiple lines of evidence suggest these phases do not impact the Mo isotope compositions of our samples. The lack of correlation between $\delta^{98/95}$Mo and TiO_2 (Fig. S5c) likely rules out influence by titanite fractionation. In addition, titanite crystallizes relatively late in a cooling magma despite being a common accessory phase in Archean granitoids (e.g., Moyen, 2020), such that crystallinity and melt viscosity considerations render segregation from the melt unlikely (e.g., Michael, 1984; Lee and Morton, 2015; Bachmann and Huber, 2019). Therefore, like other minerals, titanite directly reflects magma chemistry. Likewise, correlations between $\delta^{98/95}$Mo and TiO_2 and Nb/La are absent (Fig. S5c–d), demonstrating that Fe/Ti oxides cannot explain the variability of $\delta^{98/95}$Mo in our samples. Furthermore, Yang et al. (2015) observed no resolvable effects on Mo isotopes from Ti-magnetite fractionation in the dry Hekla suite in Iceland. However, it remains unknown whether this holds for crustal settings.

5.4. Source controls on Mo isotope compositions

Having found no evidence of control by fluid or magmatic processes, we interpret the Mo isotope compositions of our granitoids in terms of their sources. Grouping our samples by the affinity of their source protoliths, following the classification of Laurent et al. (2014), reveals a systematic relationship between $\delta^{98/95}$Mo and inferred source composition (Fig. 5), with $\delta^{98/95}$Mo increasing as the source becomes more primitive (from felsic crust to mafic crust to mantle-like; Spearman on ordinal ranks: $\rho = 0.62$, $p < 0.001$, $n = 27$). Differences between magmatic series exhibit a similar trend (from TTG through sanukitoids to potassic granitoids; Spearman on ordinal ranks: $\rho = 0.42$, $p = 0.028$, $n = 28$), consistent with source composition rather than magmatic lineage being the dominant control. Notably, a similar, albeit inverse, trend distinguishing "mafic" versus "felsic" sources is observed in Zn isotopes from granitoids from the northern Kaapvaal Craton, where TTGs and sanukitoids derived from mafic/mantle sources generally have lighter δ^{66}Zn than potassic granitoids derived from felsic crustal sources (Doucet et al., 2018, 2020). The petrogenesis of each magmatic series nonetheless involves a mixture of sources, a continuum that reflects the heterogeneous nature of the crust from which TTGs and potassic granitoids are derived and the degree of interaction between this crust and metasomatized mantle-derived magmas that produces sanukitoids and their hybrids (e.g., Moyen, 2011, 2020; Laurent et al., 2014). This continuum is expressed in the $\delta^{98/95}$Mo overlap between source affinity groups (Fig. 5) and between the contours of pure magmatic series end-members in Fig. 2c. Because each series draws on a range of protoliths rather than one, series-based groupings resolve isotopic variation less clearly than source-based groupings. The source affinity scheme is therefore better understood as identifying the dominant component in a mixture of sources than as a discrete classification, and it appears to

control the Mo isotope composition of the magmas.

5.4.1. Crustally-derived granitoids

For crustally-derived Archean granitoids, the balance in the source protolith between major elements K, Na and Ca and trace elements Rb and Sr is the dominant control on the compositional variability that encompasses the TTG-potassic granitoid magmatic spectrum (e.g., Moyen, 2011, 2020; Nebel et al., 2018; Vandenburg et al., 2023a). Moyen (2011, 2020) proposed a compositional spectrum where melting of basaltic amphibolites produces sodic TTG magmas, melting of leucoamphibolites/diorites produces "enriched TTGs" (Champion and Smithies, 2019) with higher K than regular TTGs, melting of gray gneiss/tonalite produces "ordinary" potassic granites, and melting of clay-rich metasediments produces K-rich two-mica granites. Owing to the composite nature expected of source regions, this is a simplification; many of these compositions can also be produced by a mixture of sources and melts (Moyen, 2020), particularly "enriched TTGs", which have been hypothesized in the Zimbabwe Craton to arise from the involvement of a TTG crust-derived melt phase (Rollinson et al., 2024). Nevertheless, it conceptually illustrates the source effect on the compositional variability of Archean magmas.

The Mo isotope signatures of our samples indicate a strong compositional control related to the balance of alkali and alkaline earth metals (Fig. 6). In the crustally-derived granitoids, $\delta^{98/95}$Mo shows strong negative associations with Rb/Sr, K_2O/CaO, and the modified alkali-lime index (MALI; $K_2O + Na_2O - CaO$; Frost et al., 2001; Fig. 6a–c). The previously noted decrease in $\delta^{98/95}$Mo with SiO_2 might instead suggest a differentiation control. However, this relationship is not resolved once K_2O/CaO is held constant (partial $\rho = 0.27$, $p = 0.26$), whereas the relationship with K_2O/CaO persists when SiO_2 is held constant (partial $\rho = -0.55$, $p = 0.013$), and the same asymmetry holds for Rb/Sr (Table S4). Source composition therefore accounts for the apparent silica dependence rather than the opposite. In Archean granitoids, MALI, K_2O/CaO, and Rb/Sr increase as their source becomes more enriched/evolved (Fig. 8a–b, S10a). Similar, albeit weaker, trends are observed in granitoids from the Gangdese Belt (Fan et al., 2022, 2025), the North Qilian Orogen (Chen et al., 2022a), and the Himalayan Block (Fan, 2021). Fan et al. (2021, 2022) suggest that the trends observed in their data, including a positive association between $\delta^{98/95}$Mo and europium anomaly (Eu/Eu*), result from feldspar dissolution in the source during partial melting. Given the moderate positive correlation between $\delta^{98/95}$Mo and Eu/Eu* for our samples (Fig. 7a), feldspar in the source must exert some control on the Mo isotope composition of Archean granitoids. However, the dominant mineralogical controls on the Ca-Na-K budget vary with source.

Although feldspar (and to a lesser extent, micas) control the budget of these elements in felsic and pelitic source rocks, in metabasalts other minerals play a predominant role; for Ca, amphibole is the predominant host, along with garnet (depending on the pressure of melting); for Na, amphibole and clinopyroxene are the predominant hosts; and for K, amphibole and micas are the predominant hosts. Given the purported, albeit debated (i.e., Chen et al., 2022a), role of amphibole and biotite in fractionating Mo isotopes (Voegelin et al., 2014; Wille et al., 2018), the associations discussed above cannot be solely ascribed to feldspar, as suggested by the moderate negative correlation of $\delta^{98/95}$Mo with Th/La (Fig. 7b). Other minerals such as amphibole, biotite and garnet are also likely to impact the Mo isotope composition of granitoid, but isolating their effect in our sample set is difficult.

The lack of experimental constraints on $\delta^{98/95}$Mo mineral-melt fractionation means we cannot accurately model Mo isotope behavior during the partial melting of crustal lithologies. However, we can indirectly assess the effects of changes in melt and source composition and source mineralogy by employing geochemical proxies correlated with $\delta^{98/95}$Mo in our granitoids. To further elucidate and verify the mineralogical and compositional source controls influencing the Mo isotope systematics of granitoids, we simulated partial melting of a variety of sources along multiple geothermal gradients using MAGEMin (Riel et al., 2022), allowing us to calculate the major and trace element compositions of the resultant magmas. The modeled starting materials range from juvenile metabasalts and enriched *meta*-mafic lithologies to intermediate and felsic lithologies (Table S5). For the mafic and intermediate lithologies, we assumed fractional melting conditions with a 7 vol.% critical melt connectivity threshold (Rosenberg and Handy, 2005; Huang et al., 2020) along 50, 75, and 100 °C/kbar gradients, with H_2O mostly set to minimal excess (1.5 wt.% following Hernández-Uribe, 2024). For felsic protoliths, we assumed isobaric equilibrium melting at 4, 6, and 8 kbar with H_2O set to LOI of these lithologies (<1 wt.%). The *Supplementary Information* provides a full description of the modeling methods and rationale. We provide the results in Tables S5–S8, pressure–temperature pseudosections for equilibrium melting in Figs. S6–S7, and melting path modebox plots for predicted phases in Figs. S8–S9.

Irrespective of the pressure of melting, as the starting protolith becomes increasingly enriched/evolved (i.e., mafic amphibolite vs felsic gray gneiss), the mean, median and interquartile range values of the resultant modeled melts across realistic degrees of melting (10–40 wt.%)

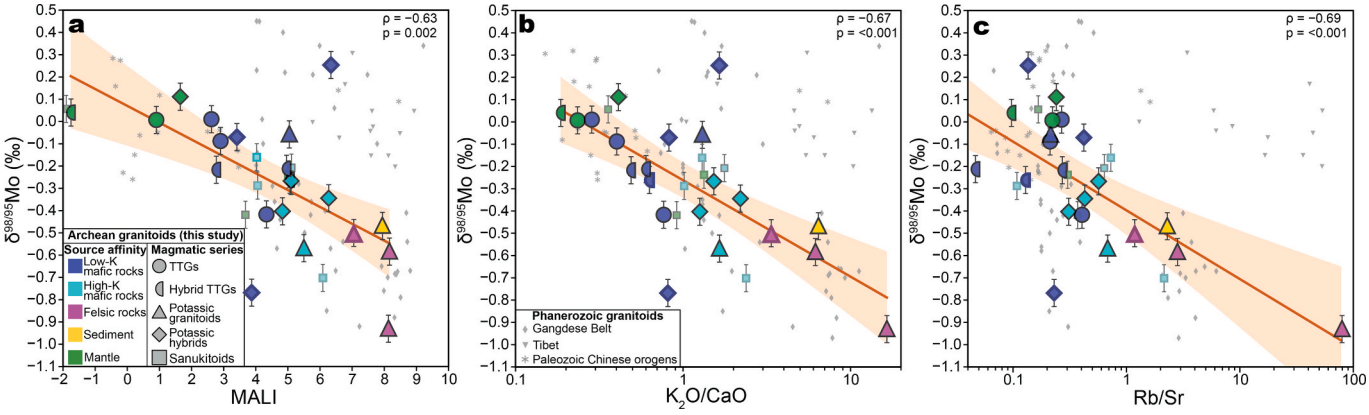


Fig. 6. Source compositional control related to the balance of alkali and alkaline earth metals strongly influences the Mo isotope signatures of Archean crustally-derived granitoids and their hybrids. Plots of $\delta^{98/95}$Mo vs the modified alkali-lime index (MALI; $K_2O + Na_2O - CaO$; Frost et al., 2001) (a), K_2O/CaO (b), and Rb/Sr (c). Also plotted for comparison are Archean sanukitoids and samples from Phanerozoic granitoid suites in the Gangdese Belt (Fan et al., 2022, 2025), the North Qilian Orogen (Chen et al., 2022a), and the Himalayan Block (Tibet; Fan, 2021). Solid orange lines and shaded areas represent the robust linear regression line and corresponding 2 se confidence envelope for crustally-derived granitoids (i.e., non-sanukitoids; $n = 21$). Also provided are Spearman's ρ and p-values for the crustally-derived Archean granitoids.

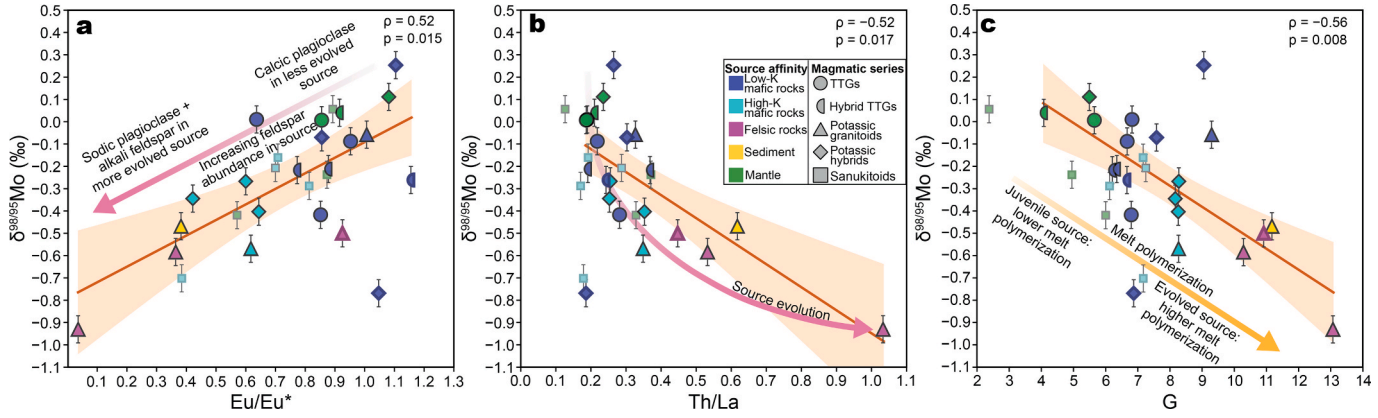


Fig. 7. Associations between $\delta^{98/95}$Mo and potential proxies of source evolution/enrichment and melt structure in Archean granitoids. Plots of $\delta^{98/95}$Mo vs europium anomaly (Eu/Eu*) (a), Th/La (b), and the compositional parameter of polymerization, G (Gervasoni et al., 2016) (c). The solid orange lines and shaded areas are robust linear regression lines and corresponding 2 se confidence envelopes for crustally-derived granitoids (i.e., non-sanukitoids; $n = 21$). Spearman's ρ and p-values for the crustally-derived Archean granitoids are also provided. The $\delta^{98/95}$Mo-Th/La relationship is marginal when sample 169044 is excluded (p = 0.053; Table S4).

show progressive increases in K_2O/CaO, Rb/Sr (Fig. 8a–b) and to a lesser degree, MALI (Fig. S10a) and a progressive decrease in Eu/Eu* (Fig. 8c). The directions of the trends in these parameters agree with their observed associations with $\delta^{98/95}$Mo (Figs. 6, 7) and suggest that the Mo isotope composition of granitoids become progressively lighter as the source becomes more evolved. This relationship is also supported by an increase in the fractional crystallization and melting-insensitive enrichment parameter ΔTh (Th [ppm] − [0.5 SiO_2 {wt.%} − 20]; Moyen et al., 2009) in the models with increasing degrees of source evolution (Fig. 8e). Although melt enrichment is affected by the starting compositions of the protoliths themselves, the magnitude of the differences between protoliths, particularly for Rb/Sr and Eu/Eu*, is relatively small. Thus, source mineralogy must also play a role by dictating the melt's chemical composition, itself dictated by the source's chemical composition. Indeed, in the models, this source evolution is accompanied by an increase in the mean and median modal weight of feldspar in the source (solely plagioclase for all except felsic lithologies) and a decrease in the mean and median anorthite content of plagioclase (Fig. S11a–b). This suggests that feldspar abundance and composition act to amplify these compositional differences between sources.

On the other hand, mean and median Th/La in the melt increase in our models as the initial source evolves from mafic to felsic (Fig. 8d), in agreement with the hypothesized role of source evolution in producing the negative correlation between $\delta^{98/95}$Mo and Th/La (Fig. 7b). Furthermore, in our compiled geochemical dataset of granitoids from the Pilbara and Yilgarn cratons, the differences in Th/La between groups supports the assertion that it is an effective discriminant of source affinity and can differentiate between TTG and potassic series magmas (Fig. S12a–b), which are higher in the latter. This increase appears to be controlled by differences in Th/La between the protoliths themselves, which is higher in more evolved/enriched sources.

Due to differences in residue mineralogy, which in turn result from compositional differences, melts derived from evolved/enriched protoliths exhibit a higher degree of polymerization. This is demonstrated by the increase in the melt compositional parameter G ($[3\ Al_2O_3 + SiO_2]/[Na_2O + K_2O + CaO + MgO + FeO]$; Gervasoni et al., 2016), which describes the degree of polymerization of the melt, as observed in our models (Fig. 8f). When calculated for our samples, $\delta^{98/95}$Mo shows a moderate negative correlation with G (Fig. 7c). This suggests that melt structure exerts a direct control on the Mo isotope systematics of granitoids. Equilibrium stable isotope fractionation is governed by the principle that heavier isotopes are preferentially incorporated into phases with the stiffest, and therefore strongest, bonds (Bigeleisen and Mayer, 1947; Urey, 1947), which form around atoms with the lowest coordination and highest valence state (Schauble, 2004). Molybdenum exists as Mo^{6+} in terrestrial silicate phases under redox conditions applicable to the upper mantle and crust (Holzheid et al., 1994; Willbold and Elliott, 2017), so high-temperature Mo isotope fractionation is coordination-dependent. Molybdenum in silicate melts is generally tetrahedrally-coordinated, existing as molybdate anions ($Mo[IV]O_4^{2-}$; Candela and Holland, 1984; Holzheid et al., 1994; Farges et al., 2006a, b). However, petrological experiments suggest that octahedrally-coordinated Mo ($Mo[VI]O_6^{6-}$) may also be present in high-SiO_2 magmas due to their highly polymerized nature, and their high volatile content may even increase the stability of Mo^{4+} (Farges et al., 2006a, b; Fan et al., 2022). This would enable the melt to preferentially incorporate light Mo isotopes during partial melting of evolved, silicic sources, which are then retained during fractional crystallization of mineral phases. Fan et al. (2022) proposed that this shift in melt coordination from tetrahedral to octahedral could explain the light $\delta^{98/95}$Mo observed in Himalayan granites, resulting from the fractional crystallization of less polymerized magma. We take this one step further and suggest that this shift can be an inherent characteristic of the parental melt, depending on the source.

Because G omits H_2O, which depolymerizes melts, and Ti, whose effect is variable (e.g., Russell et al., 2006; Mysen and Richet, 2019), we also calculated a modified non-bridging oxygen to tetrahedra ratio incorporating both (NBO/$T_{hydrous}$; Tables S7 and S8). It yields the same trend as G, becoming more polymerized as the source evolves (Fig. S10b), indicating that the trend is not an artifact of how G is calculated. With this parameter, however, it may partly reflect the assumptions about water saturation used in the starting compositions of our models, which reflect the current understanding of Archean granitoid petrogenesis (e.g., Johnson et al., 2021; Hernández-Uribe, 2024; Laurent et al., 2024). Further investigation of this concept will nonetheless require experimental studies. While largely outside the scope of this study, we briefly discuss the speculative effects of fluid activity during melting in the Supplementary Discussion.

5.4.2. *Sanukitoids*

Sanukitoids differ from crustally-derived TTG and potassic granitoids in that they come from metasomatized mantle sources, typically via interaction between mantle peridotite and crustally-derived melts, followed by evolution toward granitic compositions (e.g., Martin et al., 2005; Martin et al., 2009; Laurent et al., 2013; Moyen, 2020). The $\delta^{98/95}$Mo of Pilbara and Yilgarn sanukitoids overlaps with Cenozoic adakites, particularly on the lighter side of the distribution, whereas Cenozoic high-Mg andesites (HMAs) are generally heavier than Archean sanukitoids at comparable SiO_2 (Fig. 5). Although these Phanerozoic analogs are volcanic and not strictly equivalent to Archean plutonic

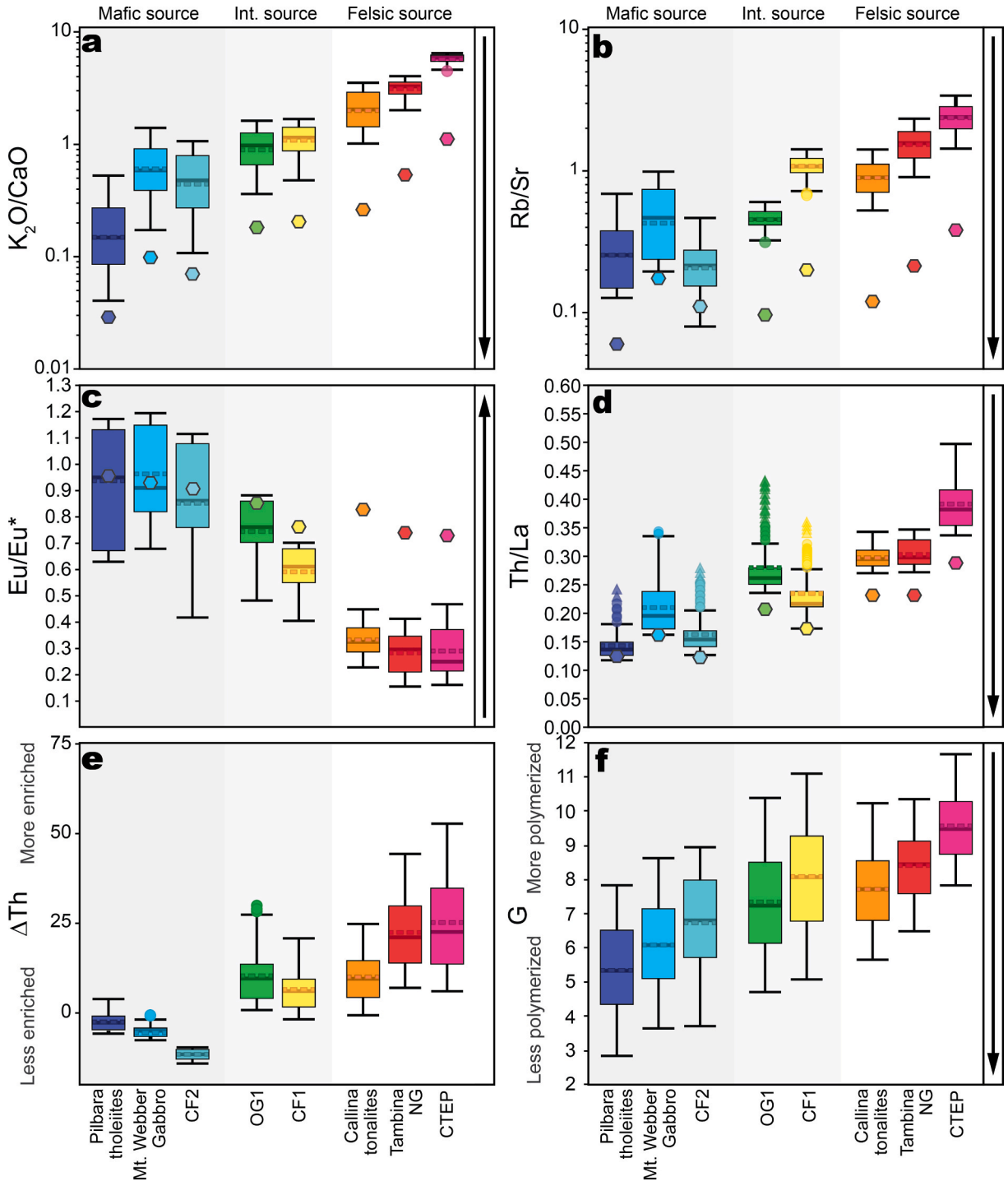


Fig. 8. Modeled variations in $\delta^{98/95}$Mo-correlated geochemical proxies as a function of of source enrichment/evolution. Box-and-whisker plots of K_2O/CaO (a), Rb/Sr (b), Eu/Eu* (c), Th/La (d), ΔTh (Th [ppm] – [0.5 SiO_2 {wt.%} – 20]; Moyen et al., 2009) (e), and compositional parameter G (f) of realistic melt fractions (10–40 wt.%) from a selection of mafic, intermediate and felsic protoliths across all P-T gradients. The box on each group defines the 25th–75th percentiles (IQR), while the enclosed solid and dashed lines denote the median and mean values, respectively. Whiskers are 1.5 times the IQR, and filled circles denote outliers. Hexagons denote parameter values for each protolith before melting, and arrows denote the direction of increasing $\delta^{98/95}$Mo observed in Archean granitoids. The starting materials modeled range from juvenile metabasalts (average Pilbara tholeiite – Smithies et al., 2021), enriched metamafic lithologies (Mount Webber Gabbro – Petersson et al., 2019; Coucal Basalt [CF2] – Johnson et al., 2017), intermediate lithologies (CF1 – Smithies et al., 2019a; OG1 – Vandenburg et al., 2023a) and through to felsic lithologies (average Callina Supersuite tonalite, average non-granitic Tambina Supersuite granitoids [Tambina NG], average pre-Cleland Supersuite felsic crust, [composite Callina-Tambina-Emu Pool – CTEP] – Vandenburg et al., 2023a).

sanukitoids, they provide a useful reference frame for interpreting Mo isotope systematics.

Only one sanukitoid in our dataset is primitive ($SiO_2 < 58$ wt.%, MgO > 5.5 wt.%; Spencer et al., 2024). This sample (235918, Central Pilbara Tectonic Zone, c. 2.95 Ga) has the heaviest $\delta^{98/95}$Mo of the series (0.06‰) and is part of the Mallina high-Mg diorite suite. Smithies and Champion (2000) modeled this suite as melts derived from a mantle source metasomatized by TTG-like slab-derived melts, which is

consistent with our observation that 235918 has Mo isotope compositions resembling older granitoids with mantle or low-K mafic crustal source affinities (Fig. 4c). In contrast, modern low-Si adakites that tap slab-melt metasomatized mantle typically have light $\delta^{98/95}$Mo, reflecting prior loss of heavy Mo in slab fluids (e.g. Ahmad et al., 2021; Liu et al., 2024). One possible explanation is a difference in slab redox: reduced Archean oceanic crust would have limited Mo loss and isotopic fractionation during slab dehydration, producing slab melts with comparatively heavy, unfractionated $\delta^{98/95}$Mo. Modern arcs where reduced sediments suppress Mo isotope fractionation during subduction offer some support for this (e.g., Freymuth et al., 2016; Gaschnig et al., 2017; Ahmad et al., 2022, 2023), but with a single primitive sanukitoid available, further studies are needed to test this hypothesis.

More evolved sanukitoids show $\delta^{98/95}$Mo values that range from slightly supra- to strongly subchondritic. They show geochemical variations, for example, differing MgO/TiO_2 ratios, that suggest varying degrees of source metasomatism relative to degrees of melting (*F/a*; Fig. 9a; e.g., Moyen, 2009). However, this is not correlated with $\delta^{98/95}$Mo (Fig. 9b), suggesting that metasomatism relative to melting is not an important control on their isotopic compositions, or at least is obscured. However, the sanukitoids share several covariations in $\delta^{98/95}$Mo and elemental parameters with their crustally-derived counterparts, such as the positive association with Eu/Eu* and the negative associations with Rb/Sr, K_2O/CaO, and MALI (Fig. 6a–c, 7a). This suggests that the same aspects of melt structure that govern the Mo isotope compositions of crustally-derived granitoids also control the compositions of sanukitoids. Another possibility is that the sanukitoid source material exhibits substantial isotopic heterogeneity, resulting in a larger spread in $\delta^{98/95}$Mo. Disentangling source and differentiation requires experimental constraints on Mo elemental and isotopic partitioning and a more in-depth study, similar to work by Spencer et al. (2024) on Ti isotopes.

5.5. Crustal evolution

Having established that source characteristics, rather than open-system or internal magmatic processes, govern the Mo isotope signatures of Archean granitoids, we can use $\delta^{98/95}$Mo as a tracer of source character and, by extension, of the degree of crustal reworking. The clearest expression of this trend is a systematic decrease in concentration-weighted $\delta^{98/95}$Mo with increasingly evolved source affinity: from mantle-derived (-0.16 ± 0.35‰; 95% CI, $n = 6$), through low-K mafic rock-derived (-0.34 ± 0.36‰; $n = 10$) and high-K mafic rock-derived (-0.38 ± 0.19‰; $n = 8$), to felsic igneous rock-derived granitoids (-0.76 ± 2.04‰; $n = 3$; the large uncertainty reflects the small effective sample size). We attribute this trend to source mineralogy, particularly the balance and presence of feldspars, along with contributions from amphibole, garnet and biotite, and to the resulting melt polymerization, which together govern Mo isotope compositions in Archean granitoids. Therefore, $\delta^{98/95}$Mo can provide an independent record of how reworked a granitoid's source is, a control also operating in Phanerozoic granitoids (Fig. S13).

The observed decrease in $\delta^{98/95}$Mo with increasing source evolution/enrichment and towards more granitic compositions aligns with established multistage models of protocraton development (e.g., Smithies et al., 2005; Van Kranendonk et al., 2015; Chowdhury et al., 2021; Smit et al., 2024; Zoleikhaei et al., 2025). In the first stage, infracrustal melting of hydrated metabasalt generates TTGs once a mafic–ultramafic plateau exceeds a critical thickness (Johnson et al., 2017) in response to volcanic resurfacing (Fig. 10a–b). These TTGs tend to have chondritic to suprachondritic $\varepsilon Hf_{(t)}$, indicating provenance from chondritic mantle-derived juvenile (basaltic) material with short crustal residence times (e.g., Petersson et al., 2020; Salerno et al., 2021; Kemp et al., 2023). The derivation from rapidly reworked juvenile material is also evidenced in the heavy $\delta^{98/95}$Mo of TTGs, which has a concentration-weighted mean of -0.11 ± 0.49‰ (95% CI, $n = 4$); note that the large uncertainty results from the small sample size. This is also observed more broadly from the more juvenile crustal source-derived granitoids (Fig. 5), in particular for the concentration-weighted mean of composite hybrid and non-hybrid TTGs (-0.12 ± 0.16‰; 95% CI, $n = 8$), and to a lesser extent, the granitoids belonging to the low-K mafic rock source affinity group. Exceptions exist, however, such as potassic granite sample 235954 (−0.58‰) from the 3.47 Ga Homeward Bound Granite of the Callina Supersuite in the Pilbara Craton, likely produced by low-degree melting (Gardiner et al., 2018) or fractionation owing to its $\varepsilon Hf_{(t)}$ slightly above CHUR (average 0.2; Kemp et al., 2023). Thus, because $\delta^{98/95}$Mo appears to decrease as the number of reworking events increases, these first-stage magmas are closest in composition to the source components

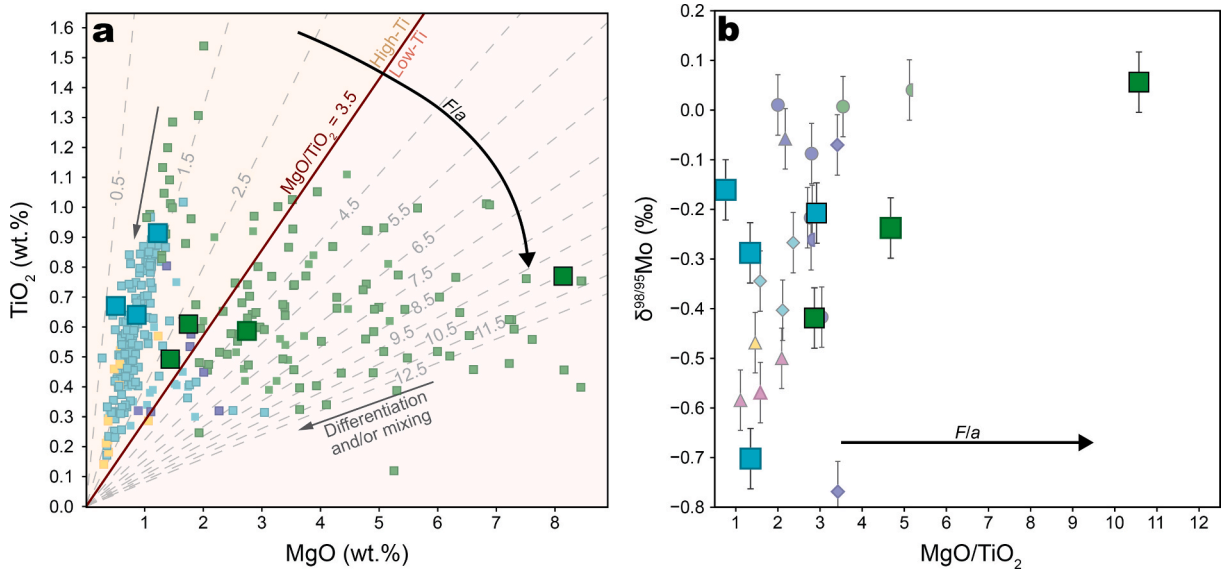
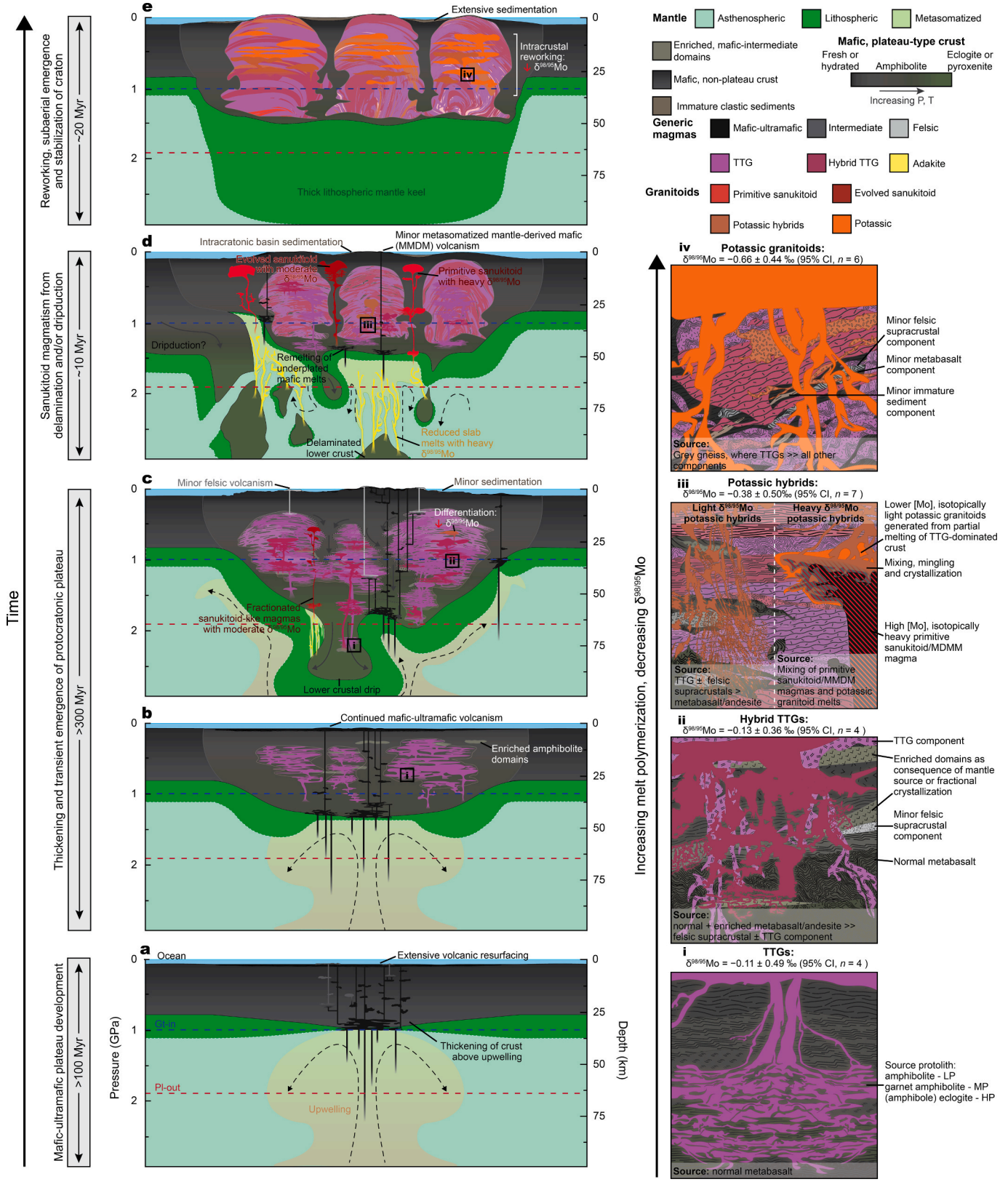


Fig. 9. No apparent control by melting/metasomatism ratios on the $\delta^{98/95}$Mo of Archean sanukitoids. (a) TiO_2 vs MgO diagram of compiled sanukitoids from the Pilbara (Vandenburg et al., 2023a) and Yilgarn (Lowrey et al., 2023) cratons illustrating the subdivision of sanukitoids into high- and low-Ti subsets and how MgO/TiO_2 (dashed lines) is controlled by the ratio of *F*, the degree of melting, to *a*, the amount of metasomatic component. Note that MgO/TiO_2 remains relatively constant during evolution and crustal contamination. (b) Plot of $\delta^{98/95}$Mo vs MgO/TiO_2 illustrating the apparent lack of influence that F/a plays on the Mo isotope compositions of sanukitoids. Symbology as for previous figures.



(caption on next page)

Fig. 10. Schematic of granitoid magmatism and Mo isotope systematics during the evolution of an Archean craton. Extensive subaqueous basaltic (± komatiitic) volcanism from upwelling asthenospheric mantle thickens the mafic protocrust into a mafic–ultramafic plateau with enriched domains (a). This plateau eventually reaches sufficient thickness (~30 km) for the occurrence of intracrustal melting of metabasalt, producing early TTGs (b). TTGs (i) have the heaviest Mo isotope compositions of the five magmatic series. (c) Further resurfacing thickens the crust, increasing the pressures at which crustal melting occurs, producing TTGs with potentially lighter Mo isotope compositions and generating dense and unstable restites at the base of the crust that begin to founder into the asthenosphere as drips. These drips form the source of TTGs, which ascend through the crust and the peripheral mantle, which may metasomatize the mantle and produce melts that fractionate to form evolved sanukitoid-like magmas with moderate $\delta^{98/95}$Mo. Melting of enriched metabasalt/andesite incorporated into greenstone packages produces hybrid TTGs (ii). (d) Adakitic melts produced from the melting of either a dripducting "slab" or the sinking into the asthenosphere of delaminated restitic lower crustal sections (these are not mutually exclusive) react with the surrounding mantle. Decompression melting of upwelling metasomatized mantle in areas of foundering generates primitive sanukitoids with comparatively heavy $\delta^{98/95}$Mo, which can evolve towards moderate $\delta^{98/95}$Mo. Around the same time, potassic hybrid granitoids (iii) appear, the product of interaction between fractionated sanukitoids/metasomatized mantle-derived mafic melts and granitic crustal melts (heavy $\delta^{98/95}$Mo) or interactions between purely crustal-derived melts (moderate to light $\delta^{98/95}$Mo). (e) Shallow intracrustal partial melting of composite gray gneiss due to upwellings or perturbation of crustal geotherms in response to post-delamination crustal relaxation generates potassic granites (iv) with light $\delta^{98/95}$Mo. This stage marks craton stabilization and generally coincides with the subaerial emersion of continental crust (e.g., Chowdhury et al., 2021, 2025). Navy blue and red dashed lines approximate the garnet-in and plagioclase-out isograds from Johnson et al. (2017). Values provided are Mo concentration-weighted means.

driving the craton's evolution: the basalts forming the initial plateau (Fig. 10a–c).

The second-stage magmas, sanukitoids, are the most restricted stage in a craton's evolution, both volumetrically and temporally. Sanukitoids carry intermediate values (concentration-weighted mean: -0.29 ± 0.23‰; 95% CI $n = 7$), and we note that our Mo data do not discriminate between the subduction-like (i.e., "dripduction"; Moyen and Laurent, 2018; Vandenburg et al., 2026) and delamination (Smithies et al., 2019b) scenarios proposed for their genesis (Fig. 10d). Their evolved members have a subchondritic concentration-weighted mean $\delta^{98/95}$Mo (-0.35 ± 0.22‰; 95% CI, $n = 6$), lighter than the single primitive sample discussed in Section 5.4.2, consistent with differentiation from a metasomatized mantle source towards lighter compositions.

Potassic hybrid granitoids begin to appear contemporaneously with sanukitoids (Fig. 10d). Their large spread in $\delta^{98/95}$Mo (concentration-weighted mean: -0.38 ± 0.50‰; 95% CI, $n = 7$) likely testifies to their varied origins (e.g., Champion and Sheraton, 1997; Laurent, 2012; Laurent et al., 2014). At least some potassic hybrids with relatively heavy $\delta^{98/95}$Mo may have been produced by interactions between fractionated sanukitoids or metasomatized mantle-derived mafic melts (comparatively high [Mo], heavy $\delta^{98/95}$Mo) and granitic crustal melts (low [Mo], light $\delta^{98/95}$Mo) (Fig. 10, inset iii). Conversely, interactions between purely crustal-derived melts may explain potassic hybrids with light $\delta^{98/95}$Mo.

The third stage of magmatic activity, potassic granitoids, largely originates from shallow intracrustal partial melting of composite gray gneisses comprised of interleaved, multiphase TTGs and minor volcanic rocks and sediments, characterized by long crustal residence times in $\varepsilon Hf_{(t)}$ (e.g., Nebel et al., 2018; Mole et al., 2019; Moyen, 2020; Chowdhury et al., 2021; Moyen et al., 2021b; Zoleikhaei et al., 2025). The concentration-weighted mean $\delta^{98/95}$Mo for potassic granitoids (-0.66 ± 0.44‰; 95% CI, $n = 6$) indicates that reworking of these composite gray gneisses produces magmas with very light Mo isotopes (Fig. 10e). These ultralight Mo isotope compositions are similar in range to granitoids from modern collisional orogens, such as the Gangdese Belt (Fan et al., 2022, 2025); we stress that this should not be used as evidence to support the operation of modern-style collisional tectonics in the Archean. As with most cratons, granitoids with sediment source affinities are rare in the Pilbara and Yilgarn cratons (Fig. 2c), and S-type granites are arguably nonexistent (Smithies et al., 2025), with exceptions in the Superior Craton (Bucholz and Spencer, 2019). Recent work by Ding et al. (2025) shows that many Himalayan leucogranites are derived from reworked igneous crust despite being commonly classified as S-types. Therefore, source evolution likely explains the commonality between Archean high-K granites and their isotopically analogous Cenozoic counterparts.

Taken together, the diversification and reworking of granitoid sources reach a common result: Archean continental crust with bulk $\delta^{98/95}$Mo similar to the modern depleted mantle, clustering around the reservoir with heavier values in samples with more mafic sources, and lighter values towards more evolved sources. Throughout a craton's lifecycle, crustal reworking produces magmas with progressively lighter Mo isotopes, reflecting evolving sources in granitoid petrogenetic environments. Because TTGs with mafic source affinities are likely more abundant than felsic-sourced potassic granitoids (e.g., Moyen, 2020), the average Archean crust, considered together with greenstone-belt mafic volcanic rocks, probably lies within the uncertainty of chondritic or depleted-mantle values (−0.14 to −0.22‰; McCoy-West et al., 2019; Hin et al., 2022). The mass balance between these source types is unknown; we therefore do not attempt to calculate a true Archean crustal value.

Under the crustal extraction hypothesis of McCoy-West et al. (2019) as the cause of the subchondritic $\delta^{98/95}$Mo of the Archean mantle as sampled by komatiites, the average $\delta^{98/95}$Mo of Archean TTGs necessitates an even larger volume of crustal extraction during the Hadean-Eoarchean for their model to remain viable. This demand may be unrealistic, instead lending weight to the crustal recycling model of Hin et al. (2022) or the delamination model of Tian et al. (2025). However, the former does not consider the consequences of crustal recycling on mantle radiogenic isotope compositions and extensive crustal recycling on the required scale is unlikely before 3.5 Ga. Nevertheless, discriminating among these will require Mo isotope data for typical Archean basalts.

6. Conclusion

We present high-precision whole-rock Mo isotope data for 28 granitoids emplaced between 3.52 and 2.63 Ga from the Australian Pilbara and Yilgarn cratons. Their $\delta^{98/95}$Mo spans from −0.93 to +0.25‰, within the range observed in Mo isotopes of modern terrestrial igneous reservoirs.

However, the Archean population is, on average, isotopically lighter than depleted mantle (McCoy-West et al., 2019; Hin et al., 2022) or chondrite. Lighter isotope values than depleted mantle develop during reworking of TTGs, but this intracrustal genesis means they do not reflect mantle isotope compositions. Crucially, the data show no secular trend from 3.52 to 2.63 Ga, either within individual cratons or combined, pointing towards petrogenetic processes as the key driver of isotopic variability. Major- and trace-element considerations, along with thermodynamic modeling, suggest that Mo isotopes in Archean granitoids primarily fingerprint source composition and mineralogy.

As cratons mature, juvenile crust-derived TTG magmatism gives way to sanukitoid magmatism linked to mantle metasomatism, and finally to potassic granitoid magmatism sourced from the reworking of TTG-dominated composite gray gneiss, a pattern mirrored by progressively lighter $\delta^{98/95}$Mo in granitoids. These results have two immediate implications. First, granitoid Mo isotope budgets evolve toward values lighter than modern DMM as crustal sources become more evolved, implying that intracrustal reworking alone can push continental

averages to sub-mantle values. As the genesis is independent of the mantle, no immediate effect on mantle values is expected. Second, attempts to resolve the origin of the Archean (upper) mantle's sub-chondritic $\delta^{98/95}$Mo cannot rely solely on granitoids. A decisive test requires Mo isotope measurements on coeval Archean basalts to establish the contemporaneous mantle signal, alongside targeted high-temperature experiments to quantify how melting conditions and source mineralogy affect Mo isotope partitioning.

Data availability

Data are available through Mendeley Data at https://doi.org/10.17632/mbbp64vdxp.1.

CRediT authorship contribution statement

Eric D. Vandenburg: Writing – original draft, Visualization, Project administration, Methodology, Investigation, Formal analysis, Data curation, Conceptualization. **Oliver Nebel:** Writing – review & editing, Validation, Supervision, Resources, Methodology, Funding acquisition, Conceptualization. **Laura M. Spencer:** Writing – review & editing, Methodology, Conceptualization. **Marc-Alban Millet:** Writing – review & editing, Resources. **R. Hugh Smithies:** Writing – review & editing, Supervision, Resources. **Peter A. Cawood:** Writing – review & editing, Supervision, Resources, Funding acquisition. **Alexandra Churchus:** Writing – review & editing, Formal analysis. **Wenli Liang:** Writing – review & editing, Formal analysis. **Emilie Bruand:** Writing – review & editing, Resources. **Jean-François Moyen:** Writing – review & editing, Resources. **Alex McCoy-West:** Writing – review & editing, Resources. **Priyardarshi Chowdhury:** Writing – review & editing, Resources.

Declaration of competing interest

The authors declare that they have no known competing financial interests or personal relationships that could have appeared to influence the work reported in this paper.

Acknowledgments

We thank Associate Editor Julie Prytulak and three anonymous reviewers for their thoughtful and thorough feedback that significantly improved the quality of our manuscript. We thank J. Lowrey for coordinating laboratory analyses of major and trace elements for the collected samples. E.D.V. acknowledges support from Australian Research Council grant IC230100035, in addition to a Graduate Scholarship and Postgraduate Publication Award from Monash University. O. N. acknowledges support from DFG Heisenberg grant 533104367. P.A. C. acknowledges support from Australian Research Council grant FL160100168. P.C. acknowledges support from DAE through NISER project grant RNI4011. R.H.S. publishes with the permission of the Executive Director of the Geological Survey of Western Australia.

Appendix A. Supplementary material

Supplementary material to this article can be found online at https://doi.org/10.1016/j.gca.2026.10.009.

References

Ahmad, Q., Wille, M., König, S., Rosca, C., Hensel, A., Pettke, T., Hermann, J., 2021. The molybdenum isotope subduction recycling conundrum: a case study from the Tongan subduction zone, Western Alps and Alpine Corsica. Chem. Geol. 576.

Ahmad, Q., Wille, M., Labidi, J., König, S., Devey, C., Mezger, K., 2023. Heavy Mo isotope enrichment in the Pitcairn plume: implications for the subduction cycle of anoxic sediments. Earth Planet. Sci. Lett. 624, 118466.

Ahmad, Q., Wille, M., Rosca, C., Labidi, J., Schmid, T., Mezger, K., König, S., 2022. Molybdenum isotopes in plume-influenced MORBs reveal recycling of ancient anoxic sediments. Geochemical Perspect. Lett. 23, 43–48.

Archer, C., Vance, D., 2008. The isotopic signature of the global riverine molybdenum flux and anoxia in the ancient oceans. Nat. Geosci. 1, 597–600.

Audétat, A., Edmonds, M., 2020. Magmatic-hydrothermal fluids. Elements 16, 401–406.

Bachmann, O., Huber, C., 2016. Silicic magma reservoirs in the Earth's crust. Am. Mineral. 101, 2377–2404.

Bachmann, O., Huber, C., 2019. The inner workings of crustal distillation columns; the physical mechanisms and rates controlling phase separation in silicic magma reservoirs. J. Petrol. 60, 3–18.

Bau, M., 1996. Controls on the fractionation of isovalent trace elements in magmatic and aqueous systems: evidence from Y/Ho, Zr/Hf, and lanthanide tetrad effect. Contrib. to Mineral. Petrol. 123, 323–333.

Bezard, R., Fischer-Gödde, M., Hamelin, C., Brennecka, G.A., Kleine, T., 2016. The effects of magmatic processes and crustal recycling on the molybdenum stable isotopic composition of mid-ocean ridge basalts. Earth Planet. Sci. Lett. 453, 171–181.

Bezard, R., Guo, H., 2023. Fluid-melt Mo isotope fractionation: implications for the $\delta^{98/95}$Mo of the upper crust. Geochemical Perspect. Lett. 26, 25–30.

Bezard, R., Rushmer, T., Turner, S., Eroglu, S., 2023. The role of exsolved fluids on the mo isotopic composition of arc lavas: insights from the adakitic rocks of solander volcano. Geochemistry Geophys. Geosystems 24, 1–19.

Bigeleisen, J., Mayer, M.G., 1947. Calculation of equilibrium constants for isotopic exchange reactions. J. Chem. Phys. 15, 261.

Bucholz C. E. (2025) The diversity and origin of granites. In *Treatise on Geochemistry* (eds. A. D. Anbar and D. Weis). Elsevier. pp. 153–202.

Bucholz, C.E., Spencer, C.J., 2019. Strongly peraluminous granites across the archean-proterozoic transition. J. Petrol. 60, 1299–1348.

Burkhardt, C., Hin, R.C., Kleine, T., Bourdon, B., 2014. Evidence for Mo isotope fractionation in the solar nebula and during planetary differentiation. Earth Planet. Sci. Lett. 391, 201–211.

Candela, P.A., Holland, H.D., 1984. The partitioning of copper and molybdenum between silicate melts and aqueous fluids. Geochim. Cosmochim. Acta 48, 373–380.

Cawood, P.A., Chowdhury, P., Mulder, J.A., Hawkesworth, C.J., Capitanio, F.A., Gunawardana, P.M., Nebel, O., 2022. Secular evolution of continents and the earth system. Rev. Geophys. 60.

Cawood, P.A., Hawkesworth, C.J., Pisarevsky, S.A., Dhuime, B., Capitanio, F.A., Nebel, O., 2018. Geological archive of the onset of plate tectonics. Philos. Trans. R. Soc. A Math. Phys. Eng. Sci. 376.

Cawood, P.A., Korsch, R.J., 2008. Assembling Australia: proterozoic building of a continent. Precambr. Res. 166, 1–35.

Champion, D.C., Sheraton, J.W., 1997. Geochemistry and Nd isotope systematics of Archaean granites of the Eastern Goldfields, Yilgarn Craton, Australia: implications for crustal growth processes. Precambr. Res. 83 (1–3), 109–113.

Champion D. C., Smithies R. H. (2001) Archean granites of the Yilgarn and Pilbara cratons, Western Australia. In: Cassidy K.F., Dunphy J.M., Van Kranendonk M.J. (Eds.), *4th International Archean Symposium 2001, Extended Abstracts, AGSO-geoscience Australia* **Record 2001/37**. 134-136.

Champion D. C. and Smithies R. H. (2019) Geochemistry of Paleoarchean Granites of the East Pilbara Terrane, Pilbara Craton, Western Australia. In *Earth's Oldest Rocks* (eds. M. J. Van Kranendonk, V. C. Bennett, and J. E. Hoffmann). Elsevier B.V. pp. 487–518.

Chatterjee, S., Ravindran, A., Ahmad, Q., Pandey, O.P., Wille, M., Mezger, K., 2025. Coeval formation of continental crust and cratonic mantle facilitated by surface material recycling in the Paleoarchean: constraints from molybdenum isotopes. Earth Planet. Sci. Lett. 654, 119227.

Chen, S., Hin, R.C., John, T., Brooker, R., Bryan, B., Niu, Y., Elliott, T., 2019. Molybdenum systematics of subducted crust record reactive fluid flow from underlying slab serpentine dehydration. Nat. Commun. 10.

Chen, S., Niu, Y., Gong, H., Wang, X., Xue, Q., 2022a. Re-assessment of the effect of fractional crystallization on Mo isotopes: constraints from I-type granitoids and their enclosed mafic magmatic enclaves. Chem. Geol. 597, 120814.

Chen, S., Sun, P., Niu, Y., Guo, P., Elliott, T., Hin, R.C., 2022b. Molybdenum isotope systematics of lavas from the East Pacific rise: constraints on the source of enriched mid-ocean ridge basalt. Earth Planet. Sci. Lett. 578, 117283.

Chen, Z., Teng, F.Z., Stern, R.J., Zhang, Y., Li, J., Zeng, Z., 2025. Molybdenum isotope evidence for subduction-modified mantle beneath mid-ocean ridges. Earth Planet. Sci. Lett. 658, 119294.

Chowdhury, P., Cawood, P.A., Mulder, J.A., 2025. Subaerial emergence of continents on Archean Earth. Annu. Rev. Earth Planet. Sci. 1–36.

Chowdhury, P., Mulder, J.A., Cawood, P.A., Bhattacharjee, S., Roy, S., Wainwright, A.N., Nebel, O., Mukherjee, S., 2021. Magmatic thickening of crust in non–plate tectonic settings initiated the subaerial rise of Earth's first continents 3.3 to 3.2 billion years ago. Proc. Natl. Acad. Sci. 118, 1–8.

Clemens, J.D., 1984. Water contents of silicic to intermediate magmas. Lithos 17, 273–287.

Clemens, J.D., Stevens, G., 2016. Melt segregation and magma interactions during crustal melting: breaking out of the matrix. Earth-Science Rev. 160, 333–349.

Deng, G.X., Kang, J.T., Nan, X.Y., Li, Y.L., Guo, J.H., Ding, X., Huang, F., 2021. Barium isotope evidence for crystal-melt separation in granitic magma reservoirs. Geochim. Cosmochim. Acta 292, 115–129.

Ding, H., Zhang, Z., Kohn, M.J., 2025. Himalayan "S-type" granite generated from I-type sources. Proc. Natl. Acad. Sci. 122, 2017.

Dolejš, D., Zajacz, Z., 2018. Halogens in silicic magmas and their hydrothermal systems. In: Harlov, D.E., Aranovich, L.Y. (Eds.), *The Role of Halogens in Terrestrial and Extraterrestrial Geochemical Processes*. Springer, Cham, pp. 431–543.

Doucet, L.S., Laurent, O., Ionov, D.A., Mattielli, N., Debaille, V., Debouge, W., 2020. Archean lithospheric differentiation: insights from Fe and Zn isotopes. Geology 48, 1028–1032.

Doucet, L.S., Laurent, O., Mattielli, N., Debouge, W., 2018. Zn isotope heterogeneity in the continental lithosphere: new evidence from Archean granitoids of the northern Kaapvaal craton, South Africa. Chem. Geol. 476, 260–271.
Fan, J.J., Wang, Q., Li, J., Wei, G.J., Ma, J.L., Ma, L., Li, Q.W., Jiang, Z.Q., Le, Z., Wang, Z.L., Long, Z., 2021. Boron and molybdenum isotopic fractionation during crustal anatexis: constraints from the Conadong leucogranites in the Himalayan Block, South Tibet. Geochim. Cosmochim. Acta 297, 120–142.
Fan, J.J., Wang, Q., Long, X.P., Wyman, D.A., Kerr, A.C., Li, J., Wang, Z.L., Gong, L., Xu, D.J., Yang, Q.J., Zhang, L., Cui, Z.X., 2025. Mo isotope evidence for the significance of subducted continental crust in formation of post-collisional porphyry Cu deposits. Chem. Geol. 680, 122683.
Fan, J.J., Wang, Q., Ma, L., Li, J., Zhang, X.Z., Zhang, L., Wang, Z.L., 2022. Extreme Mo isotope variations recorded in high-SiO_2 granites: insights into magmatic differentiation and melt–fluid interaction. Geochim. Cosmochim. Acta 334, 241–258.
Fan, J.J., Wang, Q., Wei, G.J., Li, J., Ma, L., Zhang, X.Z., Jiang, Z.Q., Ma, J.L., Zhou, J.S., Li, Q.W., Wang, Z.L., Liu, X., Huang, T.Y., Zhang, M.Y., 2023. Boron and molybdenum isotope evidence for source-controlled compositional diversity of cenozoic granites in the Eastern Tethyan Himalaya. Geochemistry, Geophys. Geosystems 24.
Fang, W., Dai, L.Q., Zhao, Z.F., 2023. Molybdenum isotopic heterogeneity for intraplate basalts and its origin. Chem. Geol. 641, 121784.
Farges, F., Siewert, R., Brown Jr, G.E., Guesdon, A., Morin, G., 2006a. Structural environments around molybdenum in silicate glasses and melts. I. Influence of composition and oxygen fugacity on the local structure of molybdenum. Can. Mineral. 44, 731–753.
Farges, F., Siewert, R., Ponader, C.W., Brown Jr, G.E., Pichavant, M., Behrens, H., 2006b. Structural environments of incompatible elements in silicate glass/melt systems. II. Effect of temperature, pressure, H_2O, halogens, and sulfur. Can. Mineral. 44, 755–773.
Freymuth, H., Elliott, T., van Soest, M., Skora, S., 2016. Tracing subducted black shales in the Lesser Antilles arc using molybdenum isotope ratios. Geology 44, 987–990.
Freymuth, H., Vils, F., Willbold, M., Taylor, R.N., Elliott, T., 2015. Molybdenum mobility and isotopic fractionation during subduction at the Mariana arc. Earth Planet. Sci. Lett. 432, 176–186.
Frost, B.R., Barnes, C.G., Collins, W.J., Arculus, R.J., Ellis, D.J., Frost, C.D., 2001. A geochemical classification for granitic rocks. J. Petrol. 42, 2033–2048.
Gardiner N. J., Hickman A. H., Kirkland C. L., Lu Y., Johnson T. E. and Wingate M. T. D. (2018) New Hf isotope insights into the Paleoarchean magmatic evolution of the Mount Edgar Dome, Pilbara Craton: Implications for early Earth and crust formation processes: Geological Survey of Western Australia, Report 181, 41p.
Gardiner, N.J., Mulder, J.A., Nebel, O., Kirkland, C.L., Johnson, T.E., 2021. Palaeoarchaean TTGs of the Pilbara and Kaapvaal cratons compared; an early Vaalbara supercraton evaluated. South African J. Geol. 124, 1–16.
Gaschnig, R.M., Reinhard, C.T., Planavsky, N.J., Wang, X., Asael, D., Chauvel, C., 2017. The molybdenum isotope system as a tracer of slab input in subduction zones: an example from Martinique, lesser Antilles Arc. Geochemistry Geophys. Geosystems 18, 4674–4689.
Gaschnig, R.M., Reinhard, C.T., Planavsky, N.J., Wang, X., Asael, D., Jackson, M.G., 2021. The impact of primary processes and secondary alteration on the stable isotope composition of ocean island basalts. Chem. Geol. 581, 120416.
Geological Survey of Western Australia, Data from "Geological Survey of Western Australia Compilation of Geochronology Information, 2020". Geological Survey of Western Australia, https://dmpbookshop.eruditetechnologies.com.au/product/compilation-of-geochronology-information-2020.do. (2020).
Geological Survey of Western Australia, Data from "Geological Map of Western Australia 1:2 500 000, 2021 Update". Geological Survey of Western Australia, https://dasc.dmirs.wa.gov.au/Download/File/3470 (2021).
Gervasoni, F., Klemme, S., Rocha-Júnior, E.R.V., Berndt, J., 2016. Zircon saturation in silicate melts: a new and improved model for aluminous and alkaline melts. Contrib. to Mineral. Petrol. 171, 1–12.
Ghose, S., 1965. A scheme of cation distribution in amphiboles. Mineral. Mag. J. Mineral. Soc. 35 (269), 46-&.
Glazner, A.F., 2007. Thermal limitations on incorporation of wall rock into magma. Geology 35, 319–322.
Greaney, A.T., Rudnick, R.L., Gaschnig, R.M., Whalen, J.B., Luais, B., Clemens, J.D., 2018. Geochemistry of molybdenum in the continental crust. Geochim. Cosmochim. Acta 238, 36–54.
Greber, N.D., Pettke, T., Nägler, T.F., 2014. Magmatic-hydrothermal molybdenum isotope fractionation and its relevance to the igneous crustal signature. Lithos 190–191, 104–110.
Greber, N.D., Puchtel, I.S., Nägler, T.F., Mezger, K., 2015. Komatiites constrain molybdenum isotope composition of the Earth's mantle. Earth Planet. Sci. Lett. 421, 129–138.
Greber, N.D., Siebert, C., Nägler, T.F., Pettke, T., 2012. $\delta^{98/95}$Mo values and molybdenum concentration data for NIST SRM 610, 612 and 3134: towards a common protocol for reporting mo data. Geostand. Geoanalytical Res. 36, 291–300.
Heinrich C. A. and Candela P. A. (2013) Fluids and Ore Formation in the Earth's Crust. In *Treatise on Geochemistry: Second Edition* (eds. H. D. Holland and K. K. Turekian). Elsevier. pp. 1–28.
Hernández-Uribe, D., 2024. Generation of Archaean oxidizing and wet magmas from mafic crustal overthickening. Nat. Geosci. 17, 809–813.
Hickman, A.H., 2023. Archean evolution of the pilbara craton and fortescue basin, 1st ed. Springer International Publishing, Cham.
Hin, R.C., Hibbert, K.E.J., Chen, S., Willbold, M., Andersen, M.B., Kiseeva, E.S., Wood, B. J., Niu, Y., Sims, K.W.W., Elliott, T., 2022. The influence of crustal recycling on the molybdenum isotope composition of the Earth's mantle. Earth Planet. Sci. Lett. 595, 117760.
Hoffmann J. E., Zhang C., Moyen J.-F. and Nagel T. J. (2019) The Formation of Tonalites–Trondjhemite–Granodiorites in Early Continental Crust. In *Earth's Oldest Rocks* (eds. M. J. Van Kranendonk, V. C. Bennett, and J. E. Hoffmann). Elsevier B.V. pp. 133–168.
Hofmann, A.W., 1988. Chemical differentiation of the Earth: the relationship between mantle, continental crust, and oceanic crust. Earth Planet. Sci. Lett. 90, 297–314.
Holness, M.B., 2018. Melt segregation from silicic crystal mushes: a critical appraisal of possible mechanisms and their microstructural record. Contrib. Miner. Petrol. 173, 48.
Holzheid, A., Borisov, A., Palme, H., 1994. The effect of oxygen fugacity and temperature on solubilities of nickel, cobalt, and molybdenum in silicate melts. Geochim. Cosmochim. Acta 58, 1975–1981.
Huang, G., Palin, R., Wang, D., Guo, J., 2020. Open-system fractional melting of Archean basalts: implications for tonalite–trondhjemite–granodiorite (TTG) magma genesis. Contrib. to Mineral. Petrol. 175, 1–25.
Irber, W., 1999. The lanthanide tetrad effect and its correlation with K/Rb, Eu/Eu*, Sr/Eu, Y/Ho, and Zr/Hf of evolving peraluminous granite suites. Geochim. Cosmochim. Acta 63, 489–508.
Ishikawa, Y., Sawaguchi, T., Iwaya, S., Horiuchi, M., 1976. Delineation of prospecting targets for Kuroko deposits based on modes of volcanism of underlying dacite and alteration haloes. Min. Geol. 26, 105–117.
Jochum, K.P., Weis, U., Schwager, B., Stoll, B., Wilson, S.A., Haug, G.H., Andreae, M.O., Enzweiler, J., 2016. Reference values following ISO guidelines for frequently requested rock reference materials. Geostand. Geoanalytical Res. 40, 333–350.
Johnson, T., Yakymchuk, C., Brown, M., 2021. Crustal melting and suprasolidus phase equilibria: from first principles to the state-of-the-art. Earth-Science Rev. 221, 103778.
Johnson, T.E., Brown, M., Gardiner, N.J., Kirkland, C.L., Smithies, R.H., 2017. Earth's first stable continents did not form by subduction. Nature 543, 239–242.
Kamber, B.S., Ossa Ossa, F., 2025. Evolution of continental crust and sedimentary rock chemistry through time. In: Anbar, A.D., Weis, D. (Eds.), Treatise on Geochemistry. Elsevier, pp. 729–773.
Kaufmann, A.K.C., Pettke, T., Wille, M., 2021. Molybdenum isotope fractionation at upper-crustal magmatic-hydrothermal conditions. Chem. Geol. 578, 120319.
Kemp, A.I.S., Vervoort, J.D., Petersson, A., Smithies, R.H., Lu, Y., 2023. A linked evolution for granite-greenstone terranes of the Pilbara Craton from Nd and Hf isotopes, with implications for Archean continental growth. Earth Planet. Sci. Lett. 601, 117895.
Kendall, B., Dahl, T.W., Anbar, A.D., 2017. The stable isotope geochemistry of molybdenum. Rev. Mineral. Geochemistry 82, 683–732.
König, S., Wille, M., Voegelin, A., Schoenberg, R., 2016. Molybdenum isotope systematics in subduction zones. Earth Planet. Sci. Lett. 447, 95–102.
Korenaga J. and Spencer C. J. (2025) An evaluation of continental growth and early Earth tectonics: Observations and models. In *Treatise on Geochemistry* (eds. A. D. Anbar and D. Weis). Elsevier. pp. 699–727.
Large, R.R., Gemmell, J.B., Paulick, H., Huston, D.L., 2001. The alteration box plot: a simple approach to understanding the relationship between alteration mineralogy and lithogeochemistry associated with volcanic-hosted massive sulfide deposits. Econ. Geol. 96, 957–971.
Laurent, O., 2012. Les changements géodynamiques à la transition Archéen-Protérozoïque: étude des granitoïdes de la marge Nord du craton du Kaapvaal (Afrique du Sud). Université Blaise Pascal - Clermont-Ferrand II.
Laurent, O., Doucelance, R., Martin, H., Moyen, J.-F., 2013. Differentiation of the late-Archaean sanukitoid series and some implications for crustal growth: insights from geochemical modelling on the Bulai pluton, Central Limpopo Belt, South Africa. Precambr. Res. 227, 186–203.
Laurent, O., Guitreau, M., Bruand, E., Moyen, J.F., 2024. At the dawn of continents: archean Tonalite-Trondhjemite-granodiorite suites. Elements 20, 174–179.
Laurent, O., Martin, H., Moyen, J.F., Doucelance, R., 2014. The diversity and evolution of late-Archean granitoids: evidence for the onset of "modern-style" plate tectonics between 3.0 and 2.5 Ga. Lithos 205, 208–235.
Laurent, O., Zeh, A., Brandl, G., Vezinet, A., Wilson, A., 2019. Granitoids and greenstone belts of the pietersburg block—witnesses of an archaean accretionary orogen along the northern edge of the kaapvaal craton. In: Kröner, A., Hofmann, A. (Eds.), *The Archaean Geology of the Kaapvaal Craton, Southern Africa*. Springer International Publishing, Cham, pp. 83–107.
Lee, C.T.A., Bachmann, O., 2014. How important is the role of crystal fractionation in making intermediate magmas? Insights from Zr and P systematics. Earth Planet. Sci. Lett. 393, 266–274.
Lee, C.T.A., Morton, D.M., 2015. High silica granites: terminal porosity and crystal settling in shallow magma chambers. Earth Planet. Sci. Lett. 409, 23–31.
Lipp, A.G., Shorttle, O., Sperling, E.A., Brocks, J.J., Cole, D.B., Crockford, P.W., Del Mouro, L., Dewing, K., Dornbos, S.Q., Emmings, J.F., Farrell, U.C., Jarrett, A., Johnson, B.W., Kabanov, P., Keller, C.B., Kunzmann, M., Miller, A.J., Mills, N.T., O'Connell, B., Peters, S.E., Planavsky, N.J., Ritzer, S.R., Schoepfer, S.D., Wilby, P.R., Yang, J., 2021. The composition and weathering of the continents over geologic time. Geochemical Perspect. Lett. 17, 21–26.
Liu, H.-Q., Li, J., Xu, Y.-G., Yumul, G.P., Knittel, U., Dimalanta, C.B., Payot, B.D., Queaño, K., Huang, X.-L., Zhang, L., 2023. Heavy Mo isotope composition of northern Bataan adakites, Philippines: evidence for fore-arc subduction erosion? Geology 51, 49–53.
Liu, H.Q., Tian, F., Hoernle, K., Li, J., Huang, X.L., Zhang, L., Bindeman, I., Xu, Y.G., 2024. Molybdenum isotope insights into recycling of wedge serpentinite and fore-arc crust in subduction zones. Chem. Geol. 665, 122302.

Liu, P., Zhang, J., Ding, X., Liu, Y., Li, T., 2026. Tracing Mesoarchean crust-mantle interaction processes using Mo–Sr–Nd–Hf isotopes in TTGs and Nb-enriched basalts in the Kongling complex, Yangtze Craton. Chem. Geol. 714, 123446.
Louvel, M., Sanchez-Valle, C., Malfait, W.J., Cardon, H., Testemale, D., Hazemann, J.-L., 2014. Constraints on the mobilization of Zr in magmatic-hydrothermal processes in subduction zones from in situ fluid-melt partitioning experiments. Am. Mineral. 99, 1616–1625.
Lowrey, J.R., Smithies, R.H., Champion, D.C., Cassidy, K.F., 2023. Systematic classification of Yilgarn Craton granitic rocks. Geol. Surv. West. Aust. Rep. 12, 1–27.
Ma, L., Xu, Y.-G., Li, J., Chen, L.-H., Liu, J.-Q., Li, H.-Y., Huang, X.-L., Ma, Q., Hong, L.-B., Wang, Y., 2022. Molybdenum isotopic constraints on the origin of EM1-type continental intraplate basalts. Geochim. Cosmochim. Acta 317, 255–268. https://doi.org/10.1016/j.gca.2021.11.013.
Martin, H., Moyen, J.F., Rapp, R., 2009. The sanukitoid series: magmatism at the Archaean-Proterozoic transition. Earth Environ. Sci. Trans. R. Soc. Edinburgh 100, 15–33.
Martin, H., Smithies, R.H., Rapp, R., Moyen, J.-F., Champion, D., 2005. An overview of adakite, tonalite–trondhjemite–granodiorite (TTG), and sanukitoid: relationships and some implications for crustal evolution. Lithos 79, 1–24.
McCoy-West, A.J., Chowdhury, P., Burton, K.W., Sossi, P., Nowell, G.M., Fitton, J.G., Kerr, A.C., Cawood, P.A., Williams, H.M., 2019. Extensive crustal extraction in Earth's early history inferred from molybdenum isotopes. Nat. Geosci. 12, 946–951.
Michael, P.J., 1984. Chemical differentiation of the Cordillera Paine granite (southern Chile) by in situ fractional crystallization. Contrib. Miner. Petrol. 87, 179–195.
Mole, D.R., Kirkland, C.L., Fiorentini, M.L., Barnes, S.J., Cassidy, K.F., Isaac, C., Belousova, E.A., Hartnady, M., Thebaud, N., 2019. Time-space evolution of an Archean craton: a Hf-isotope window into continent formation. Earth-Science Rev. 196, 102831.
Morón, S., Kohn, B.P., Beucher, R., Mackintosh, V., Cawood, P.A., Moresi, L., Gallagher, S.J., 2020. Denuding a craton: thermochronology record of phanerozoic unroofing from the Pilbara Craton, Australia. Tectonics 39, 1–30.
Moyen, J.-F., Janoušek, V., Laurent, O., Bachmann, O., Jacob, J.-B., Farina, F., Fiannacca, P., Villaros, A., 2021a. Crustal melting vs. fractionation of basaltic magmas: part 1, the bipolar disorder of granite petrogenetic models. Lithos.
Moyen, J.-F., 2009. High Sr/Y and La/Yb ratios: The meaning of the "adakitic signature". Lithos 112 (3-4), 556–574. https://doi.org/10.1016/j.lithos.2009.04.001.
Moyen, J.F., 2011. The composite Archaean grey gneisses: petrological significance, and evidence for a non-unique tectonic setting for Archaean crustal growth. Lithos 123, 21–36.
Moyen, J.F., 2020. Archean granitoids: classification, petrology, geochemistry and origin. Geol. Soc. Spec. Publ. 489, 15–49.
Moyen, J.F., Champion, D., Smithies, R.H., 2009. The geochemistry of Archaean plagioclase-rich granites as a marker of source enrichment and depth of melting. Earth Environ. Sci. Trans. R. Soc. Edinburgh 100, 35–50.
Moyen, J.F., Laurent, O., 2018. Archaean tectonic systems: a view from igneous rocks. Lithos 302–303, 99–125.
Moyen, J.F., Martin, H., 2012. Forty years of TTG research. Lithos 148, 312–336.
Moyen, J.F., Zeh, A., Cuney, M., Dziggel, A., Carrouée, S., 2021b. The multiple ways of recycling Archaean crust: a case study from the ca. 3.1 Ga granitoids from the Barberton Greenstone Belt, South Africa. Precambr. Res. 353.
Mysen, B., Richet, P., 2019. Silicate glasses and melts, 2nd ed. Elsevier.
Nebel, O., Capitanio, F.A., Moyen, J.F., Weinberg, R.F., Clos, F., Nebel-Jacobsen, Y.J., Cawood, P.A., 2018. When crust comes of age: on the chemical evolution of Archaean, felsic continental crust by crustal drip tectonics. Philos. Trans. R. Soc. A Math. Phys. Eng. Sci. 376.
Nebel-Jacobsen, Y., Wille, M., Ivanic, T., Nebel, O., 2021. Molybdenum isotope systematics in cumulate rock of the 2.8 Windimurra layered intrusion: a test for igneous differentiation and the composition of the Archean mantle. Precambr. Res. 355, 106087.
Neely, R.A., Gislason, S.R., Ólafsson, M., McCoy-West, A.J., Pearce, C.R., Burton, K.W., 2018. Molybdenum isotope behaviour in groundwaters and terrestrial hydrothermal systems. Iceland. Earth Planet. Sci. Lett. 486, 108–118.
Nesbitt, H.W., Young, G.M., 1982. Early Proterozoic climates and plate motions inferred from major element chemistry of lutites. Nature 299, 715–717.
O'Connor, J.T., 1965. A classification for quartz-rich igneous rocks based on feldspar ratios. U.S. Geol. Surv. Prof. Pap. 525, 79–84.
O'Neill, H.S.C., Eggins, S.M., 2002. The effect of melt composition on trace element partitioning; and experimental investigation of the activity coefficients of FeO, NiO, CoO, MoO_2 and MoO_3 in silicate melts. Chem. Geol. 186, 151–181.
Ohta, T., Arai, H., 2007. Statistical empirical index of chemical weathering in igneous rocks: a new tool for evaluating the degree of weathering. Chem. Geol. 240, 280–297.
Palin, R.M., White, R.W., Green, E.C.R., 2016. Partial melting of metabasic rocks and the generation of tonalitic–trondhjemitic–granodioritic (TTG) crust in the Archaean: constraints from phase equilibrium modelling. Precambr. Res. 287, 73–90.
Petersson, A., Kemp, A.I.S., Gray, C.M., Whitehouse, M.J., 2020. Formation of early Archean Granite-Greenstone Terranes from a globally chondritic mantle: insights from igneous rocks of the Pilbara Craton. Western Australia. Chem. Geol. 551, 119757.
Petersson, A., Kemp, A.I.S., Hickman, A.H., Whitehouse, M.J., Martin, L., Gray, C.M., 2019. A new 3.59 Ga magmatic suite and a chondritic source to the east Pilbara Craton. Chem. Geol. 511, 51–70.
Pontow, R., Bezard, R., Willbold, M., Turner, S., Di Rocco, T., 2025. Untangling the effects of crustal and source processes on the Mo isotope systematics of oceanic arcs: insights from the Tonga-Kermadec subduction system. Geochim. Cosmochim. Acta 397, 13–36.
Prytulak J. and König S. (2025) Stable isotope variations in arc lavas. In *Treatise on Geochemistry* (eds. A. D. Anbar and D. Weis). Elsevier. pp. 671–701.
Rapp, R.P., Watson, E.B., Miller, C.F., 1991. Partial melting of amphibolite/eclogite and the origin of Archaean trondhjemites and tonalites. Precambr. Res. 51, 1–25.
Riel, N., Kaus, B.J.P., Green, E.C.R., Berlie, N., 2022. MAGEMin, an Efficient Gibbs Energy Minimizer: Application to Igneous Systems. Geochem. Geophys. Geosys. 23 (7), e2022GC010427. https://doi.org/10.1029/2022gc010427.
Roberts, M.P., Clemens, J.D., 1995. Feasibility of AFC models for the petrogenesis of calc-alkaline magma series. Contrib. to Mineral. Petrol. 121, 139–147.
Rodney, J.B., Andersen, M.B., Murton, B.J., Elliott, T., 2025. Constraints from uranium and molybdenum isotope ratios on the origin of enriched mid-ocean ridge basalts. Earth Planet. Sci. Lett. 666, 119491.
Rojas-Kolomiets, E., Jensen, O., Bizimis, M., Yogodzinski, G., Ackerman, L., 2023. Serpentinite fluids and slab-melting in the Aleutian arc: evidence from molybdenum isotopes and boron systematics. Earth Planet. Sci. Lett. 603, 117970.
Rollinson, H., 2021. Do all Archaean TTG rock compositions represent former melts? Precambr. Res. 367, 106448.
Rollinson, H., Chagondah, G., Hofmann, A., 2024. The late Archaean granite paradox: a case study from the Zimbabwe Craton. Precambr. Res. 410, 107491.
Rosenberg, C.L., Handy, M.R., 2005. Experimental deformation of partially melted granite revisited: implications for the continental crust. J. Metam. Geol. 23, 19–28.
Rudge, J.F., Reynolds, B.C., Bourdon, B., 2009. The double spike toolbox. Chem. Geol. 265, 420–431.
Rudnick R. L. and Gao S. (2003) Composition of the Continental Crust. In *Treatise on Geochemistry* (eds. H. D. Holland and K. K. Turekian). Elsevier. pp. 1–64.
Russell, J.K., Giordano, D., Kopylova, M., Moss, S., 2006. Transport properties of kimberlite melt. In Long Abstract, Kimberlite Emplacement Workshop, Saskatoon, Canada.
Salerno, R., Vervoort, J., Fisher, C., Kemp, A., Roberts, N., 2021. The coupled Hf-Nd isotope record of the early Earth in the Pilbara Craton. Earth Planet. Sci. Lett. 572, 117139.
Schauble, E., 2004. Applying stable isotope fractionation theory to new systems. Rev. Mineral. Geochem. 55, 65–111.
Shannon, R.D., 1976. Revised effective ionic radii and systematic studies of interatomic distances in halides and chalcogenides. Acta Cryst 32, 751–767.
Skora, S., Freymuth, H., Blundy, J., Elliott, T., Guillong, M., 2017. An experimental study of the behaviour of cerium/molybdenum ratios during subduction: implications for tracing the slab component in the Lesser Antilles and Mariana Arc. Geochim. Cosmochim. Acta 212, 135–155.
Smit, M.A., Mezger, K., 2017. Earth's early O_2 cycle suppressed by primitive continents. Nat. Geosci. 10, 788–792.
Smit, M.A., Musiyachenko, K.A., Goumans, J., 2024. Archaean continental crust formed from mafic cumulates. Nat. Commun. 15, 692.
Smith, W.D., Jenkins, M.C., Augustin, C.T., Virtanen, V.J., Vukmanovic, Z., Driscoll, B.O., 2024. Layered intrusions in the Precambrian: observations and perspectives. Precambr. Res. 415, 107615.
Smithies, R.H., 2000. The Archaean tonalite-trondhjemite-granodiorite (TTG) series is not an analogue of Cenozoic adakite. Earth Planet. Sci. Lett. 182, 115–125.
Smithies, R.H., Champion, D.C., 2000. The Archaean high-Mg diorite suite: links to Tonalite-Trondhjemite-Granodiorite magmatism and implications for early Archaean crustal growth. J. Petrol. 41, 1653–1671.
Smithies, R.H., Lu, Y., Champion, D.C., Sweetapple, M.T., Lowrey, J.R., Bowman, N.H., Cassidy, K.F., Ivanic, T.J., Kemp, A.I.S., Turnbull, R.E., Gessner, K., Korhonen, F.J., 2025. Giant lithium-rich pegmatites in Archean cratons form by remelting refertilised roots of greenstone belts. Commun. Earth Environ. 6, 630.
Smithies, R.H., Lu, Y., Johnson, T.E., Kirkland, C.L., Cassidy, K.F., Champion, D.C., Mole, D.R., Zibra, I., Gessner, K., Sapkota, J., De Paoli, M.C., Poujol, M., 2019b. No evidence for high-pressure melting of Earth's crust in the Archean. Nat. Commun. 10, 1–12.
Smithies, R.H., Lu, Y., Kirkland, C.L., Johnson, T.E., Mole, D.R., Champion, D.C., Martin, L., Jeon, H., Wingate, M.T.D., Johnson, S.P., 2021. Oxygen isotopes trace the origins of Earth's earliest continental crust. Nature 592, 70–75.
Smithies, R.H., Van Kranendonk, M.J., Champion, D.C., 2005. It started with a plume - early Archaean basaltic proto-continental crust. Earth Planet. Sci. Lett. 238, 284–297.
Smithies R. H., Champion D. C. and Van Kranendonk M. J. (2019a) The Oldest Well-Preserved Felsic Volcanic Rocks on Earth: Geochemical Clues to the Early Evolution of the Pilbara Supergroup and Implications for the Growth of a Paleoarchean Protocontinent. In *Earth's Oldest Rocks* (eds. M. J. Van Kranendonk, V. C. Bennett, and J. E. Hoffmann). Elsevier. pp. 463–486.
Spencer, L.M., 2025. Insights into sanukitoid formation and evolution from novel stable isotope systems. Cardiff University.
Spencer, L.M., Albert, C., Williams, H.M., Nebel, O., Parkinson, I.J., Smithies, R.H., Bruno, H., Fowler, M., Moreira, H., Lissenberg, C.J., Millet, M.A., 2024. Tracing hydrous eclogite melts in the source of sanukitoids. Earth Planet. Sci. Lett. 648, 119067.
Stegner, C.J., Gaschnig, R.M., Marshall, S., Rader, S.T., Bebout, G.E., Penniston-Dorland, S.C., 2025. Molybdenum isotope behavior during subduction zone metamorphism. Geochim. Cosmochim. Acta 388, 294–306.
Tamblyn, R., Hermann, J., Hasterok, D., Sossi, P., Pettke, T., Chatterjee, S., 2023. Hydrated komatiites as a source of water for TTG formation in the Archean. Earth Planet. Sci. Lett. 603, 117982.
Tattitch, B.C., Blundy, J.D., 2017. Cu-Mo partitioning between felsic melts and saline-aqueous fluids as a function of X_{eq}^{NaCl}, fO_2, and fS_2. Am. Mineral. 102, 1987–2006.
Thomas, R., Förster, H.J., Rickers, K., Webster, J.D., 2005. Formation of extremely F-rich hydrous melt fractions and hydrothermal fluids during differentiation of highly

evolved tin-granite magmas: a melt/fluid-inclusion study. Contrib. to Mineral. Petrol. 148, 582–601.
Tian, Y., Huang, F., Xu, J., Li, J., Zeng, Y., McCoy-West, A.J., 2025. Missing molybdenum and the composition of the continental crust inferred from. Nat. Commun. 1–10.
Urey, H.C., 1947. The thermodynamic properties of isotopic substances. J. Chem. Soc. 562–581.
Van Kranendonk, M.J., Hugh, S.R., Griffin, W.L., Huston, D.L., Hickman, A.H., Champion, D.C., Anhaeusser, C.R., Pirajno, F., 2015. Making it thick: a volcanic plateau origin of Palaeoarchean continental lithosphere of the Pilbara and Kaapvaal cratons. Geol. Soc. Spec. Publ. 389, 83–111.
Vandenburg, E.D., Nebel, O., Cawood, P.A., Smithies, R.H., Capitanio, F.A., Miller, L.A., Millet, M., Bruand, E., Moyen, J.-F., Wang, X., Raveggi, M., Jacobsen, Y., 2023b. The stability of cratons is controlled by lithospheric thickness, as evidenced by Rb-Sr overprint ages in granitoids. Earth Planet. Sci. Lett. 621, 118401.
Vandenburg, E.D., Nebel, O., Smithies, R.H., Capitanio, F.A., Miller, L., Cawood, P.A., Millet, M.-A., Bruand, E., Moyen, J.-F., Wang, X., Nebel-Jacobsen, Y., 2023a. Spatial and temporal control of Archean tectonomagmatic regimes. Earth-Science Rev. 241, 104417.
Vandenburg, E.D., Nebel, O., Smithies, R.H., Cawood, P.A., Miller, L.A., Millet, M.A., Capitanio, F.A., 2026. Modern arc-like water content in the source of 3.1-billion-year-old volcanic rocks. Nat. Commun. 17.
Veevers, J.J., Saeed, A., Belousova, E.A., Griffin, W.L., 2005. U-Pb ages and source composition by Hf-isotope and trace-element analysis of detrital zircons in Permian sandstone and modern sand from southwestern Australia and a review of the paleogeographical and denudational history of the Yilgarn Craton. Earth-Science Rev. 68, 245–279.
Villalobos-Orchard, J., Freymuth, H., O'Driscoll, B., Elliott, T., Williams, H., Casalini, M., Willbold, M., 2020. Molybdenum isotope ratios in Izu arc basalts: the control of subduction zone fluids on compositional variations in arc volcanic systems. Geochim. Cosmochim. Acta 288, 68–82.
Voegelin, A.R., Pettke, T., Greber, N.D., von Niederhäusern, B., Nägler, T.F., 2014. Magma differentiation fractionates Mo isotope ratios: evidence from the Kos Plateau Tuff (Aegean Arc). Lithos 190–191, 440–448.
Weber, U.D., Kohn, B.P., Gleadow, A.J.W., Nelson, D.R., 2005. Low temperature Phanerozoic history of the Northern Yilgarn Craton, Western Australia. Tectonophysics 400, 127–151.
White, R.W., Palin, R.M., Green, E.C.R., 2017. High-grade metamorphism and partial melting in Archean composite grey gneiss complexes. J. Metam. Geol. 35, 181–195.
Whitney J. A. (1990) The origin of granite: The role and source of water in the evolution of granitic magmas. In *Centennial Articles* (eds. R. D. Hatcher Jr. and W. A. Thomas). Geological Society of America.
Wilke, M., Schmidt, C., Dubrail, J., Appel, K., Borchert, M., Kvashnina, K., Manning, C.E., 2012. Zircon solubility and zirconium complexation in $H_2O+Na_2O+SiO_2\pm Al_2O_3$ fluids at high pressure and temperature. Earth Planet. Sci. Lett. 349–350, 15–25.
Wilkinson, J.J., 2013. Triggers for the formation of porphyry ore deposits in magmatic arcs. Nat. Geosci. 6, 917–925.
Willbold, M., Elliott, T., 2017. Molybdenum isotope variations in magmatic rocks. Chem. Geol. 449, 253–268.
Willbold, M., Elliott, T., 2023. Molybdenum isotope evidence for subduction-modified, recycled mafic oceanic crust in the mantle sources of ocean island basalts from La Palma and Hawaii. Earth Planet. Sci. Lett. 621, 118399.
Willbold, M., Hibbert, K., Lai, Y.-J., Freymuth, H., Hin, R.C., Coath, C., Vils, F., Elliott, T., 2015. High-precision mass-dependent molybdenum isotope variations in magmatic rocks determined by double-spike MC-ICP-MS. Geostand. Geoanalytical Res. 40, 389–403.
Willbold, M., Messling, N., 2023. Systematic across-arc variations of molybdenum isotopes in a fluid-dominated subduction zone system. Geochemistry, Geophys. Geosystems 24.
Wille, M., Nebel, O., Pettke, T., Vroon, P.Z., König, S., Schoenberg, Ronny, 2018. Molybdenum isotope variations in calc-alkaline lavas from the Banda arc, Indonesia: Assessing the effect of crystal fractionation in creating isotopically heavy continental crust. Chem. Geol. 485, 1–13. https://doi.org/10.1016/j.chemgeo.2018.02.037.
Williams-Jones, A.E., Heinrich, C.A., 2005. 100th anniversary special paper: vapor transport of metals and the formation of magmatic-hydrothermal ore deposits. Econ. Geol. 100, 1287–1312.
Wyllie, P.J., 1979. Magmas and volatile components. Am. Mineral. 64, 469–500.
Xia, Y., Sun, G., Gao, P., Zhao, Z., Zhou, Y., Li, Z., Wen, G., Qin, L., 2025b. The dual origin of granites from fluid-absent and fluid-fluxed melting of the juvenile lower crust: new constraints from Mo isotopes and phase equilibrium modeling. Geochim. Cosmochim. Acta.
Xia, Y.-S., Gao, P., Sun, G.-C., Zhao, Z.-F., Qin, L., Wen, G., Li, Z.-X., Dai, L.-Q., 2025a. Fluid-fluxed melting of juvenile lower crust traced by molybdenum isotopes. Geology 53, 125–129.
Yang, J., Barling, J., Siebert, C., Fietzke, J., Stephens, E., Halliday, A.N., 2017. The molybdenum isotopic compositions of I-, S- and A-type granitic suites. Geochim. Cosmochim. Acta 205, 168–186.
Yang, J., Siebert, C., Barling, J., Savage, P., Liang, Y., Halliday, A.N., 2015. Absence of molybdenum isotope fractionation during magmatic differentiation at Hekla volcano. Iceland. Geochim. Cosmochim. Acta 162, 126–136.
Zack, T., Kronz, A., Foley, S.F., Rivers, T., 2002. Trace element abundances in rutiles from eclogites and associated garnet mica schists. Chem. Geol. 184, 97–122.
Zajacz, Z., Halter, W.E., Pettke, T., Guillong, M., 2008. Determination of fluid/melt partition coefficients by LA-ICPMS analysis of co-existing fluid and silicate melt inclusions: controls on element partitioning. Geochim. Cosmochim. Acta 72, 2169–2197.
Zeng, Y., Xu, J., Chen, J., Li, J., Huang, F., 2025. Tracing crustal recycling mechanisms using Mo isotopes in high-Mg andesites. Geology 53, 343–348.
Zeng, Y.C., Xu, J.F., Huang, F., Liu, X.J., Li, M.J., Huang, Q.T., Li, Z.L., 2024. Central Tibetan adakitic rocks archive the critical impact of water on the Nb/Ta variation in deep crustal melts. Geochim. Cosmochim. Acta 384, 228–241.
Zhao, X.C., Yan, S., Niu, H.C., Yang, W., Bin, L.N.B., Li, J., Zhang, L., McCoy-West, A.J., 2025. Molybdenum isotopes demonstrate that multistage upgrading is required to generate heavy rare earth element–enriched carbonatites. Bull. Geol. Soc. Am. 137, 1855–1871.
Zoleikhaei, Y., Chaudhuri, T., Cawood, P.A., Mazumder, R., Nebel, O., De, S., 2025. Magmatic maturation of Archean continental crust via a three-step crustal reworking, western Singhbhum Craton. Chem. Geol. 671, 122483.